# *In Situ* Observation of Elementary Growth Processes of Protein Crystals by Advanced Optical Microscopy

Gen Sazaki[1,†,*], Alexander E.S. Van Driessche[2], Guoliang Dai[3], Masashi Okada[1,‡], Takuro Matsui[1], Fermín Otálora[2], Katsuo Tsukamoto[4] and Kazuo Nakajima[1,¶]

[1]*Institute for Materials Research, Tohoku University, 2-1-1 Katahira, Aoba-ku, Sendai 980-8577, Japan;* [2]*Laboratorio de Estudios Crystalográficos, IACT, CSIC/UGr, Av. de las Palmeras nr°4, 18100 Armilla (Granada), Spain;* [3]*National Microgravity Laboratory, Institute of Mechanics, Chinese Academy of Sciences, No. 15, Bei Si Huan Xi Road, Beijing 100190, China;* [4]*Graduate School of Science, Tohoku University, Aza-Aoba, Aramaki, Aoba-ku, Sendai 980-8578, Japan*

*†Present address: Institute of Low Temperature Science, Hokkaido University, N19-W8, Kita-ku, Sapporo 060-0819, Japan; ‡Present address: Konica Minolta Business Technologies, Inc., 2970 Ishikawa-machi, Hachioji 192-8505, Japan; ¶Present address: Graduate School of Energy Science, Kyoto University, Yoshida-honmachi, Sakyo-ku, Kyoto 606-8501, Japan*

**Abstract:** To start systematically investigating the quality improvement of protein crystals, the elementary growth processes of protein crystals must be first clarified comprehensively. Atomic force microscopy (AFM) has made a tremendous contribution toward elucidating the elementary growth processes of protein crystals and has confirmed that protein crystals grow layer by layer utilizing kinks on steps, as in the case of inorganic and low-molecular-weight compound crystals. However, the scanning of the AFM cantilever greatly disturbs the concentration distribution and solution flow in the vicinity of growing protein crystals. AFM also cannot visualize the dynamic behavior of mobile solute and impurity molecules on protein crystal surfaces. To compensate for these disadvantages of AFM, *in situ* observation by two types of advanced optical microscopy has been recently performed. To observe the elementary steps of protein crystals noninvasively, laser confocal microscopy combined with differential interference contrast microscopy (LCM-DIM) was developed. To visualize individual mobile protein molecules, total internal reflection fluorescent (TIRF) microscopy, which is widely used in the field of biological physics, was applied to the visualization of protein crystal surfaces. In this review, recent progress in the noninvasive *in situ* observation of elementary steps and individual mobile protein molecules on protein crystal surfaces is outlined.

**Keywords:** Adsorption, advanced optical microscopy, elementary steps, impurity effect, *in situ* observation, single molecule visualization, surface diffusion, two-dimensional nucleation.

## INTRODUCTION

### A General Picture of Protein Crystal Growth

Studies on the growth mechanisms of protein crystals started in the mid-1980s. In the beginning, it was thought that crystal growth mechanisms unique to biological materials existed. However, subsequent research clarified that the crystal growth mechanisms of proteins are essentially identical to those of inorganic and low-molecular-weight compounds [1-6]. In other words, solute molecules are also incorporated into kinks on elementary steps on protein crystal surfaces (schematically shown in Fig. (**1**)). These steps are the growing ends of ubiquitous molecular layers with the minimum height determined by the size of the molecules and crystal structures. Utilizing the growth of elementary steps in the lateral directions, protein crystals grow layer by layer, as in the case of other crystals. Under low and medium supersaturation ranges, elementary steps are generated by screw dislocations and two-dimensional nucleation, while crystal surfaces become rough at the molecular level under a high supersaturation range. Hence, we can now apply the knowl-

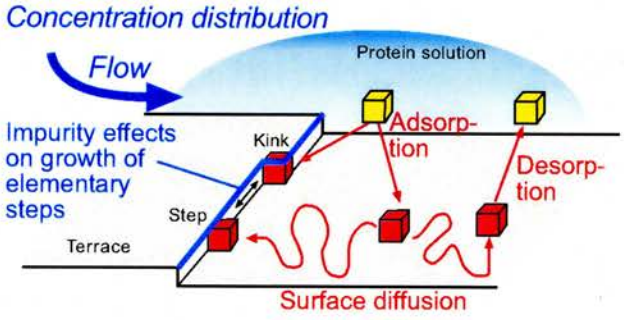


**Figure 1.** Schematic illustration of elementary growth processes of a protein crystal.

*Address correspondence to this author at the Institute of Low Temperature Science, Hokkaido University, N19-W8, Kita-ku, Sapporo 060-0819, Japan; Tel: +81-11-706-6880; Fax: +81-11-706-6880; E-mail: sazaki@lowtem.hokudai.ac.jp

1875-5305/12 $58.00+.00 

edge that was obtained from the crystal growth of inorganic and low-molecular-weight compounds to that of proteins.

To systematically investigate the quality improvement of protein crystals, two types of research must be carried out. First, we need to clarify the elementary growth processes that proceed on protein crystal surfaces. Second, we must also investigate the correlation between the X-ray diffraction properties of protein crystals and the types and distribution of lattice defects generated in protein crystals. However, the second type of research has so far been seldom performed, showing the necessity of close collaboration between the fields of crystal growth and structural biology. In this review, the recent progress in the first type of research is explained.

## Elementary Growth Processes

The growth of protein crystals includes the successive mass transfer and surface incorporation processes of solute and impurity molecules. The phenomena that have so far been clarified and those that remain unsolved are summarized in Table **1**.

Because of the mass transfer of solute molecules from a solution to a crystal, the solute concentration decreases, and hence a solute-depleted zone develops around a growing crystal [7-12]. Since this solute-depleted zone has lower density than a bulk solution, buoyancy convection arises [13, 14]. Such convection flow stirs the solution, and then enhances the mass transfer of solute and impurity molecules to the crystal surface [15-19]. The use of microgravity [15, 20-24] and gel media [25-29] significantly suppresses the convection flow and mass transfer. Depending on the balance between the mass transfer of the solute and impurity, convection flow has either a positive or negative effect on crystal quality [12]. Observation of the surface diffusion of solute and impurity molecules on a protein crystal surface was inaccessible until very recently, because of the absence of studies attempting to noninvasively observe individual mobile protein molecules on protein crystal surfaces.

On the other hand, to clarify the surface incorporation process of protein crystals, the macroscopic surface morphology and the normal growth of crystal faces were first observed by interferometry [3, 7, 30-33] and ordinary optical microscopy [9, 34, 35]. Subsequently, the direct visualization of individual elementary steps by atomic force microscopy (AFM) [1, 4, 5, 36-38], which is the most popular technique used for the *in situ* observation of solid surfaces at the molecular level, confirmed that the growth of protein crystals also involves layer-by-layer growth utilizing kinks and steps (Fig. **1**). AFM has also been used to visualize individual protein molecules that were incorporated at kink sites and in a nucleus [39-43]. However, at solution-crystal interfaces, the scanning of the AFM cantilever greatly disturbs the concentration distribution of solute/impurity molecules and the solution flow in the vicinity of the crystal surface (we will discuss this issue later in detail). AFM also cannot visualize the dynamic behavior of mobile solute and impurity molecules on protein crystal surfaces. Hence the dynamic behavior of elementary steps and mobile protein molecules must be clarified.

## *In Situ* Visualization

As summarized in Table **1**, to fully comprehend the elementary growth processes, we must visualize 1) elementary steps and 2) individual mobile protein molecules without disturbing the distribution of protein molecules and the flow in the vicinity of a growing protein crystal.

To visualize elementary steps on protein crystal surfaces, the authors and Olympus Engineering Co., Ltd., developed a method of laser confocal microscopy combined with differential interference contrast microscopy (hereafter referred to as LCM-DIM) and succeeded in their visualization for the first time [44]. Since then, the authors [45-50], Suzuki *et al.* [35, 51], and Sleutel *et al.* [52-54] have performed the *in situ* optical observation of elementary steps on protein crystals under various growth conditions.

To visualize individual solute/impurity molecules (single-molecule visualization), total internal reflection fluorescent (TIRF) microscopy, which is widely used in the field of biological physics (first report [55] and reviews [56-59]), was adopted. The authors succeeded in simulating the behavior of solute protein molecules on a protein crystal surface,

**Table 1. Growth Processes of Protein Crystals**

| Known Phenomena | Unknown Problems |
|---|---|
| *Mass transfer process*<br># Formation of solute-depleted zones<br># Generation of buoyancy convection<br># Convective flow enhances the mass transfer of solute and impurity molecules (suppression of flow suppress their mass transfer.) | # Contribution of surface diffusion of solute molecules at solution-crystal interfaces |
| *Surface incorporation process*<br># Advancement of individual steps by spiral growth and two-dimensional nucleation growth mechanisms has been visualized mainly by AFM<br># Incorporation of solute molecules at kink sites on steps has been also visualized by AFM | # Effects of the scan of a cantilever of AFM<br># Dynamic behavior of mobile solute and impurity molecules on protein crystal surfaces |

and they observed the surface diffusion and adsorption/desorption processes of individual protein molecules for the first time [60, 61].

This review mainly consists of three parts.

First, the direct optical observation of elementary steps by LCM-DIM is discussed. The advantages of the noninvasive observation and the application to the measurement of the two-dimensional nucleation rate are presented.

Second, the single-molecule visualization of individual mobile protein molecules on protein crystal surfaces is reported. Novel mechanisms found in the diffusion and adsorption/desorption processes are demonstrated.

Finally, the simultaneous observation of elementary steps and single molecules in the same field of view is explained, and we give an example of the supersaturation dependence of impurity effects.

## MATERIALS AND METHODS

The {110} faces of tetragonal crystals of hen egg-white lysozyme were observed *in situ* by LCM-DIM and single-molecule visualization that was newly devised to observe the interfaces of a solution and a protein crystal. (Fig. **2a**) shows a schematic illustration of the experimental setup.

### LCM-DIM

A confocal system (FV300, Olympus) and a diagonal illumination system using an objective were constructed on an inverted optical microscope (IX70, Olympus) [44]. A 20x objective (LUCPlan Fl 20x, Olympus) and a superluminescent diode (Amonics Ltd., model ASLD68-050-B-FA: 680 nm), whose coherent length and full width at half maximum were about 10 μm and 23 nm, respectively, were used for LCM-DIM observation of elementary steps. The use of the superluminescent diode was beneficial for removing interference fringes from LCM-DIM images.

(Fig. **2b**) presents a cross-sectional view of the observation cell (1x10x20 $mm^3$) used for observation of elementary steps. The observation cell was made of two glass plates of 0.17 mm thickness separated by 1 mm polystyrene spacers. The bold arrow in (Fig. **2b**) indicates the interface at which steps were observed by LCM-DIM.

The temperature increase by the laser irradiation could not be measured within the detection limit of ±0.05°C. Since lysozyme does not have adsorption at 680 nm, no effect was observed. If sample protein has adsorption at 680 nm, a superluminescent diode of other wavelength must be used.

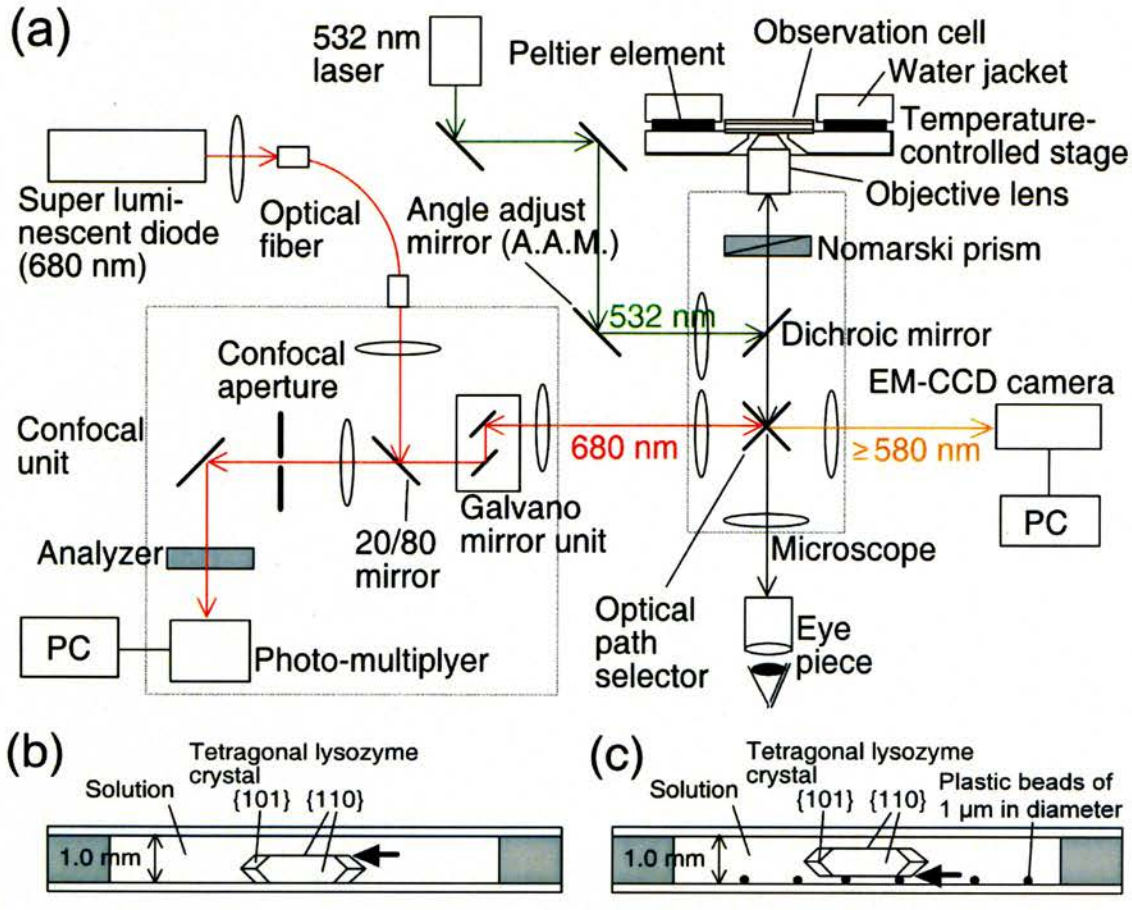


**Figure 2.** Schematic illustrations of experimental setup. (**a**) LCM-DIM, single-molecule visualization system, and temperature-controlled stage. (**b**) Cross-sectional views of observation chamber used for *in situ* observation by LCM-DIM. (**c**) Observation chamber for single-molecule visualization of an oblique illumination type. Bold arrows indicate the crystal-solution interfaces at which *in situ* observations were carried out. Reprinted with permission from the reference [48]. Copyright 2009 American Chemical Society.

### Single-molecule Visualization

A 60x oil-immersion objective (PlanApo 60xO TIRFM3, Olympus) was used for the observations of individual fluorescence-labeled lysozyme (F-lysozyme) [62] and fluorescence-labeled dimer (F-dimer) [48] molecules on the crystal surface. These fluorescence-labeled molecules were illuminated with a 532 nm laser, and emission at ≥580 nm was recorded at a frame rate of 100 ms with an electron multiplying charge-coupled device camera (EM-CCD: DV887, Andor Technology) [61]. The 60x objective was used to observe the same field of view by LCM-DIM and by single-molecule visualization.

A cross-sectional view of the observation cell (1x10x20 $mm^3$) used for the single-molecule visualization experiments is shown schematically in (Fig. **2c**). A tetragonal lysozyme crystal was placed on 1 μm spacer beads adsorbed on a bottom glass plate [61]. The solution-crystal interface (bold arrow in (Fig. **2c**)) was illuminated by a laser beam tilted almost parallel to the crystal surface to avoid an increase in the background intensity of the fluorescent light.

After the inside of the chamber was chemically washed, tetragonal lysozyme crystals (several 100 μm in height) and a solution containing 45 mg/ml lysozyme, 0.1 nM F-lysozyme, and 50 mM sodium acetate (pH 4.5) were then transferred into the chamber. The temperature of the chamber was controlled at 25.0 ± 0.1 °C, at which the crystals and the solution were in equilibrium, using Peltier elements and water jackets. Other details of the observations have been explained in our previous works [48, 60, 61].

## DIRECT OPTICAL OBSERVATION OF ELEMENTARY STEPS

We observed *in situ* the {110} and {101} faces of growing tetragonal lysozyme crystals by LCM-DIM. (Fig. **3**) shows typical examples of the observations. As shown in a sequence of micrographs, we could clearly visualize 2D islands of the elementary step height (5.6 nm for the {110} face and 3.4 nm for the {101} face [1, 2, 63, 64]) by LCM-DIM [49]. We could follow the time course of birth-and-spread type 2D nucleation growth; on the {110} face, arrows in the micrographs indicate the appearance of new 2D islands during the time intervals between consecutive images. Here, we only showed significant parts of the images, although we observed elementary steps on whole crystal surfaces. LCM-DIM could also visualize dislocations that were aligned perpendicular to the optical axis [45].

### Advantages of Optical Microscopy Measurements

Here, we emphasize the importance of noninvasive observation by optical microscopy, although AFM is the most popular type of microscopy for the observation of solid surfaces at the molecular level. Van Driessche and coworkers measured step velocities as a function of supersaturation using tapping- and contact-mode AFM in the <001> directions on {110} faces of tetragonal lysozyme (Fig. **4a**) [47]. No significant difference was observed between data obtained by these two AFM operational modes. We also measured step velocities by LCM-DIM and phase-shift Michelson interferometry (PSMI) under the same conditions, and com-

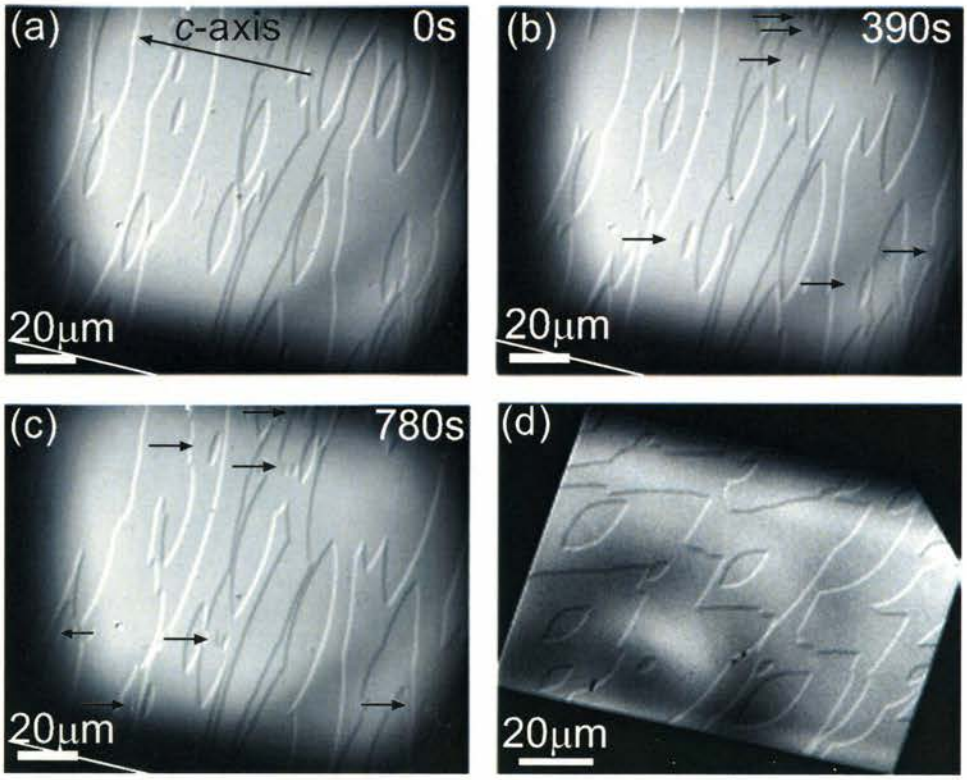


**Figure 3.** Micrographs of 2D nucleation behaviour on {110} (**a-c**) and {101} (**d**) faces of growing tetragonal lysozyme crystals, observed by LCM-DIM. The sequence of micrographs shows the time course of birth-and-spread type 2D nucleation growth: 0 s (**a**), 390 s (**b**), and 780 s (**c**). Arrows indicate the appearance of new 2D islands during the time intervals between consecutive images. Growth conditions: 56 mg/ml (**a-c**) and 40 mg/ml (**d**) 99.99% pure lysozyme, NaCl 25 mg/ml, in 50 mM sodium acetate buffer (pH 4.5), and at 22.0°C (**a-c**) and 26.0°C (**d**). Reprinted with permission from the reference [49]. Copyright 2007 American Chemical Society.

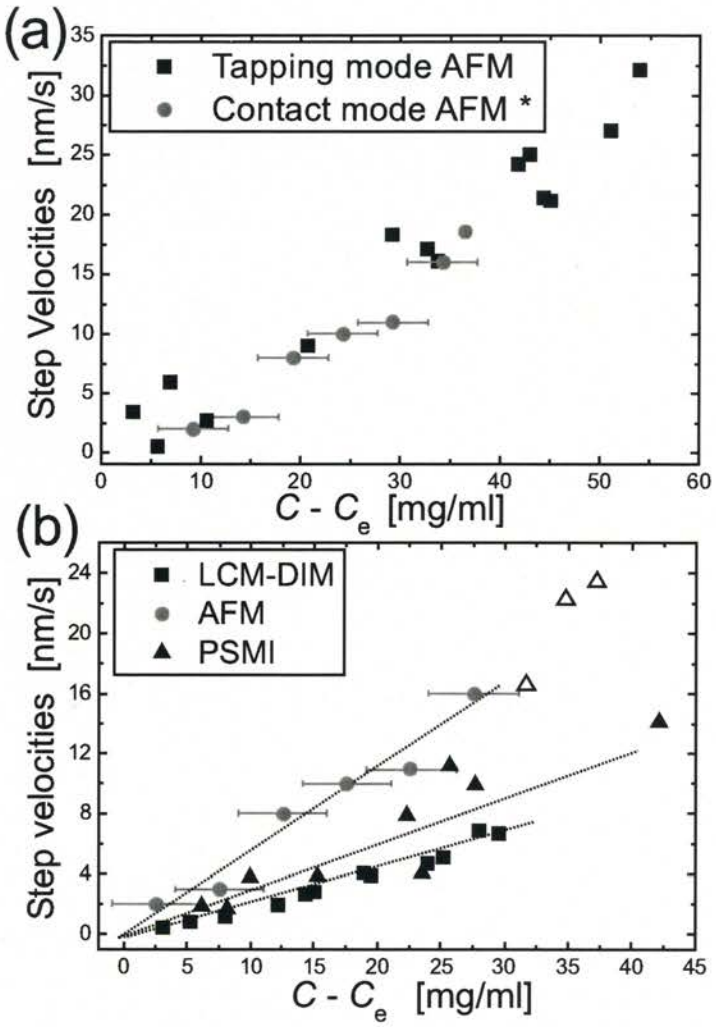


**Figure 4.** Step velocities measured in the long-axis direction (<001>) of 2D islands on {110} faces of tetragonal lysozyme crystals. (**a**) Step velocities measured by tapping- and contact-mode AFM. $C$ and $C_e$ indicate solute concentration and solubility, respectively. (**b**) Step velocities measured by AFM, LCM-DIM, and PSMI. Open triangles indicate step velocities calculated from PSMI data obtained above a critical supersaturation ($C - C_e > 30$ mg/mL) where 2D nucleation becomes important. Reprinted with permission from the reference [47]. Copyright 2008 American Chemical Society.

pared the results with those obtained by AFM. As (Fig. **4b**) shows, step velocities measured by optical techniques (LDM-DIM and PSMI) are significantly smaller than those obtained by AFM (contact mode), although the data obtained by PSMI show scattering. These results indicate that the movement of a cantilever significantly stirs the diffusion boundary layer developed in the vicinity of a growing crystal, increasing the solute concentration at the step edge and the subsequent step velocity.

The use of LCM-DIM also enabled us to observe elementary steps in gel media [46]. (Fig. **5**) presents LCM-DIM images of 2D islands on the {110} faces of tetragonal lysozyme crystals, taken without (a) and with (b-d) agarose gel. In a commercial-grade (98.5% pure) lysozyme solution, 2D islands exhibit a lens-like morphology with the ratio of the long axis to the short axis being about 2-4 (Fig. **5a**). Dold *et al.* reported that with increasing purity of a lysozyme sample, the ratio of the long to short axes increased to ~6 (in a 99.99% pure lysozyme solution) [50]. As (Fig. **5**) shows, with increasing agarose concentration, the ratio of the long to short axes also increased to about 6, demonstrating that agarose gel functioned as an impurity filter that inhibited the diffusion of impurities from a bulk solution to a crystal surface.

Suzuki *et al.* also visualized elementary steps (7.2 nm high) of glucose isomerase crystals under high pressure (50 MPa) [51], and reported that with increasing hydrostatic pressure, the crystallization of glucose isomerase is accelerated both thermodynamically and kinetically. LCM-DIM will enable the visualization of elementary steps under other extreme conditions, such as forced flow conditions, where AFM cannot function properly.

We have further kept improving the sensitivity of LCM-DIM by increasing signal-noise ratio and by improving polarization property. Consequently, LCM-DIM recently succeeded in visualizing steps of various heights on inorganic crystals: 0.76 nm (gypsum crystals in aqueous solutions) [65], 0.37 nm ($H_2O$ Ih ice crystals in air) [66, 67] and 0.25 nm (gold {111} surfaces in aqueous solutions) [68, 69], demonstrating that the detection sensitivity of LCM-DIM in

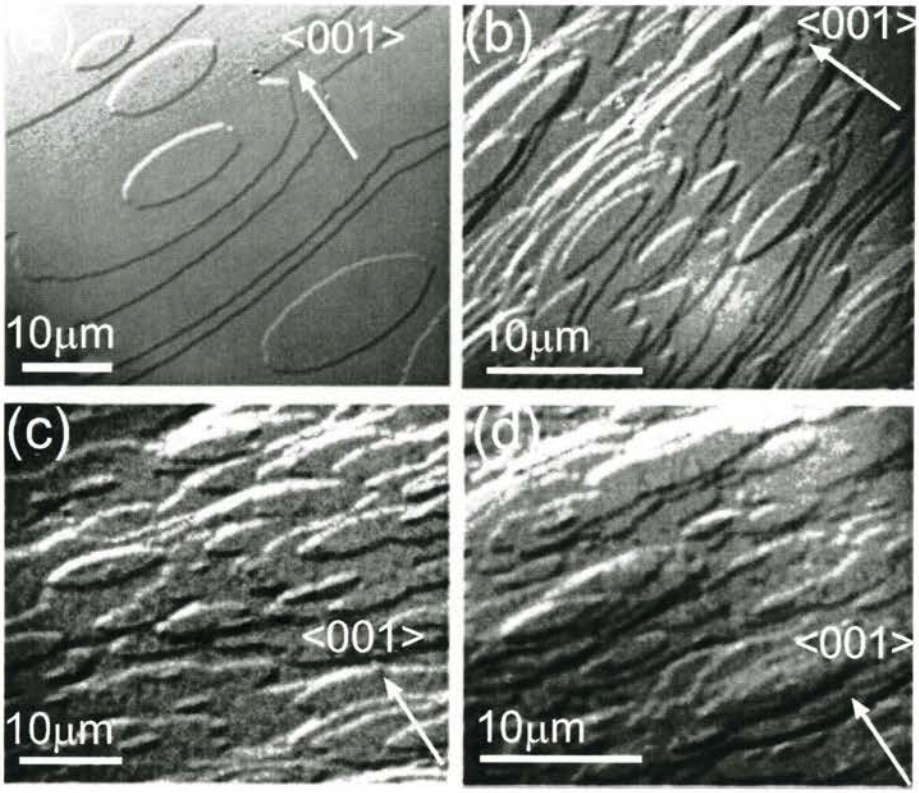


**Figure 5.** Micrographs of 2D island morphology on {110} faces of tetragonal lysozyme crystals: (**a**) no gel, (**b**) 0.075% (w/v), (**c**) 0.125% (w/v), and (**d**) 0.175% (w/v) agarose gel. Growth conditions: 40 mg/ml (**a**) and (d), 38 mg/ml (b), and 41 mg/ml (c) commercial-grade (98.5% pure) lysozyme, 25 mg/ml NaCl, in 50 mM sodium acetate buffer (pH 4.5), and at 25.0°C (**a**), 20.0°C (**b**) and (**c**), 19.0°C (**d**). Reprinted with permission from the reference [46]. Copyright 2008 American Chemical Society.

the *z* direction has truly reached molecular/atomic resolution. In contrast, in the case of transmission type optical microscopy, ordinary phase contrast microscopy can visualize elementary steps of tetragonal crystals (5.6 nm thick) [50] and even $CdI_2$ crystals (1.4 nm thick) [70], suggesting that the combination of laser confocal microscopy and phase contrast microscopy will show better sensitivity than LCM-DIM despite the smaller feasibility.

## Homogeneous and Heterogeneous Two-dimensional Nucleation

Using LCM-DIM, we carried out noninvasive observation of 2D nucleation processes on tetragonal lysozyme crystals, as demonstrated in (Fig. **3**). Then we measured the 2D nucleation rate $J$ under various conditions of supersaturation $\sigma = \ln(C/C_e)$, where $C$ is the solute concentration and $C_e$ the solubility, and also under various concentrations of impurities. All data are summarized in (Fig. **6**) [49].

Since elementary steps on the {110} faces involve two molecules per step [1, 2, 63, 64], we considered 2D nuclei composed of a double layer. By modifying the classical expression for homogenous 2D nucleation [71, 72] considering double-layered circular islands, the steady-state 2D nucleation rate, $J$, can be expressed as [71, 72]

$$\ln J = \ln(\varpi \Gamma Z) - \frac{\pi s \kappa^2}{2k_B{}^2 T^2 \ln(C/C_e)}, \quad (1)$$

where $\varpi$ is the attachment frequency of a solute molecule to a critical nucleus, $\Gamma$ the Zeldovich factor, $Z$ the 2D concentration of solute molecules on a crystal surface, $s$ the area one molecule occupies inside a nucleus ($s$=1.06x$10^{-17}$ $m^2$) [64], $\kappa$ the ledge free energy of a 2D cluster, $k_B$ the Boltzmann constant, and $T$ the absolute temperature.

(Fig. **6**) shows changes in $\ln J$ as a function of $1/[T^2 \ln(C/C_e)]$. On the {110} faces, a highly linear relationship was found for all the data points under a higher supersaturation range $\sigma$>0.80 (solid line). This result demonstrates clearly that these data can be satisfactorily expressed by Eq. (1) and that the impurities did not affect the 2D nucleation rates in this higher supersaturation range; that is, homogeneous 2D nucleation occurred. However, the plots of lysozyme with impurities exhibit a kink at intermediate supersaturation $\sigma \approx 0.80$ (arrow), leading to a line with a much smaller slope under a lower supersaturation range $\sigma$<0.80 (dash-dotted line). This smaller slope indicates the occurrence of heterogeneous 2D nucleation with smaller $\kappa$ in this lower supersaturation range. Even 99.99% pure lysozyme shows four data points (broken line) at lower supersturation $\sigma$<0.80 that deviate from the linear relationship found under the higher supersaturation range, showing that an impurity molecule concentration of less than 0.01% can influence the growth kinetics of protein crystals, as in the case of inorganic crystals. On the {101} faces, very similar results were obtained, as shown in (Fig. **6**) (solid line and dotted line).

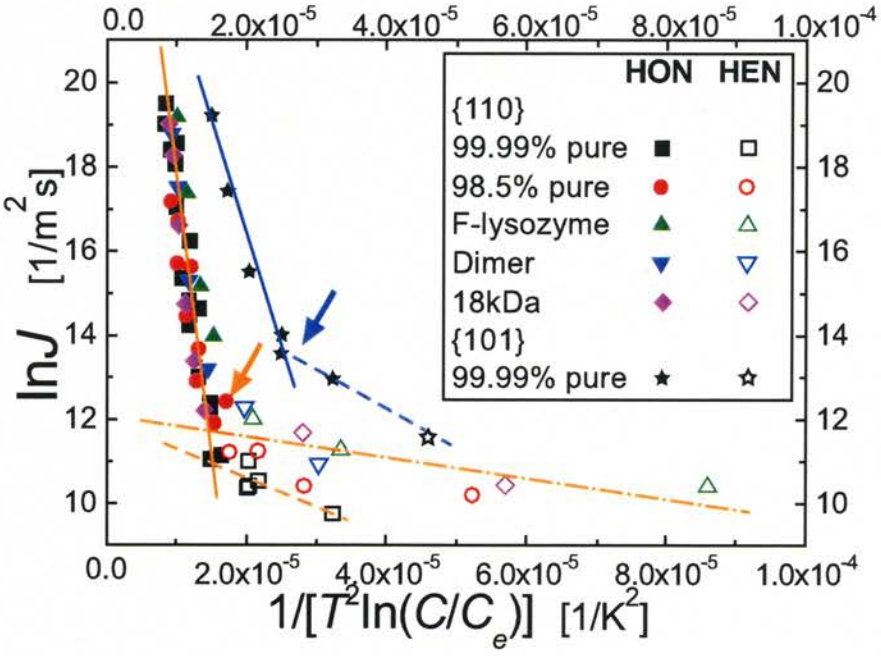


**Figure 6.** Changes in ln$J$ as a function of $1/[T^2\ln(C/C_e)]$ measured on {110} and {101} faces of tetragonal lysozyme crystals. Here, $J$ is the 2D nucleation rate, $T$ the absolute temperature, $C$ the solute concentration, and $C_e$ the solubility. HON and HEN denote homogeneous and heterogeneous nucleation, respectively. Solid lines represent homogeneous 2D nucleation under a higher supersaturation range; broken lines the heterogeneous 2D nucleation in the purified lysozyme solution under a lower supersaturation range; and the dash-dotted line the heterogeneous 2D nucleation in the solution containing impure proteins under a lower supersaturation range. Arrows show kinks at which solid and broken lines intersect each other. The impurity concentrations of F-lysozyme, dimer, and 18kDa protein molecules were 0.1%. The 98.5% pure lysozyme contained 0.5% dimer and 1.0% 18kDa protein molecules. Growth conditions: supersaturation $\sigma$=0-1.4, 25 mg/ml NaCl, in 50 mM sodium acetate buffer (pH 4.5), and at 18.0-26.0°C. Reprinted with permission from the reference [49]. Copyright 2007 American Chemical Society.

We also observed peculiar 2D nucleation events at rare intervals. Arrows in the sequence of micrographs shown in (Fig. **7**) indicate the regions in which 2D islands with their centers at the same position were generated repeatedly [49]. Note that the interstep distances of the concentric 2D islands generated repeatedly are irregular (bars in Fig. **7**). Although two screw dislocations with opposite signs can generate a similar surface structure composed of concentric islands, the irregular interstep distances clearly indicate that the 2D islands nucleated repeatedly at irregular time intervals at the same site. The repeated 2D nucleation normally continued for 3 to 4 layers and could be observed irrespective of the supersaturation. The repeated nucleation was mainly observed when impure proteins were present in the lysozyme solutions. In the case of the 99.99% pure lysozyme solution, the proportion of occasions on which we could find repeated nucleation was about 20%, but it was 60% for the solutions that contained the impurities. This is a strong indication that the impure proteins are responsible for the repeated 2D nucleation. Liu *et al.* [73] explained that any kind of foreign particle and even impurity molecule can potentially serve as a nucleation center that will promote nucleation by lowering barriers to 2D nucleation. In addition, after the impure molecules were incorporated into the crystal surface, the strain fields generated around the impurities also played an important role in lowering step-ledge free energies [71] and thus promoted the 2D nucleation repeatedly, until the effects of the strain field did not reach the crystal surface (3 to 4 layers in this study).

The sequence of micrographs in (Fig. **8**) shows 2D nucleation and the subsequent lateral growth of a multilayer island that exhibits much higher contrast than the elementary islands [49]. In (Fig. **8a**), a white arrow indicates the existence of a foreign particle on the crystal surface, since the particle did not grow at the same rate as the other islands. After 80 s (Fig. **8b**), a 2D island appeared at this foreign particle (white arrow) and a second 2D island appeared next to the first one (black arrow). After 230 s (Fig. **8c**), the first island that nucleated at the foreign particle grew over the second island (black arrowhead). This observation demonstrates that the first island had multiple layer height. Sometimes foreign particles adsorbed on a crystal surface were observed at the center of the multilayer islands. In addition, multilayer islands frequently appeared on the crystal surfaces after the replacement of the solution inside the observation chamber and also after the crystals were transferred from stock tubes of seed crystals to the observation chamber. Furthermore, no strong correlation was found between the presence of the impure proteins and the appearance of multilayer islands. Taking into account these results, we concluded that relatively large foreign particles, probably microcrystals generated by the flow and/or collision of seed crystals followed by adsorption on a crystal surface, are responsible for the formation of the multilayer islands. The relatively large height of the foreign particles is thought to have resulted in the lateral growth of the multilayer islands.

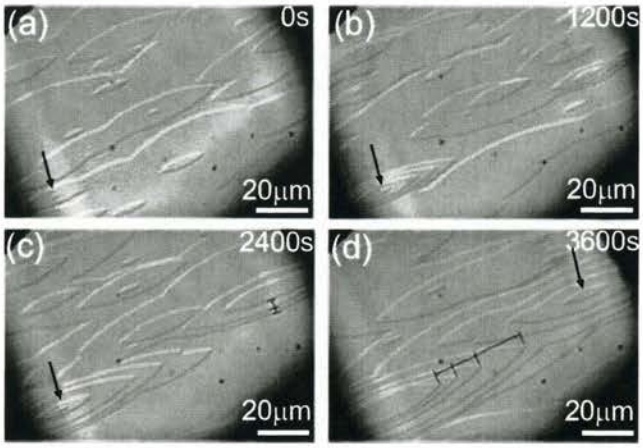


**Figure 7.** Micrographs of repeated 2D nucleation on {110} face of growing tetragonal lysozyme crystal taken by LCM-DIM. The sequence of micrographs shows the time course of repeated 2D nucleation: 0 s (**a**), 1200 s (**b**), 2400 s (**c**), and 3600 s (**d**). Black arrows show the regions in which 2D islands with their centers at the same position were generated repeatedly. The repeated 2D nucleation normally continued for 3 to 4 layers. Bars indicate that the interstep distances of the concentric 2D islands generated repeatedly are irregular. Growth conditions: 38 mg/ml 99.99% pure lysozyme, 0.05% F-lysozyme, 25 mg/ml NaCl, in 50 mM sodium acetate buffer (pH 4.5), and at 24.0℃. Reprinted with permission from the reference [49]. Copyright 2007 American Chemical Society.

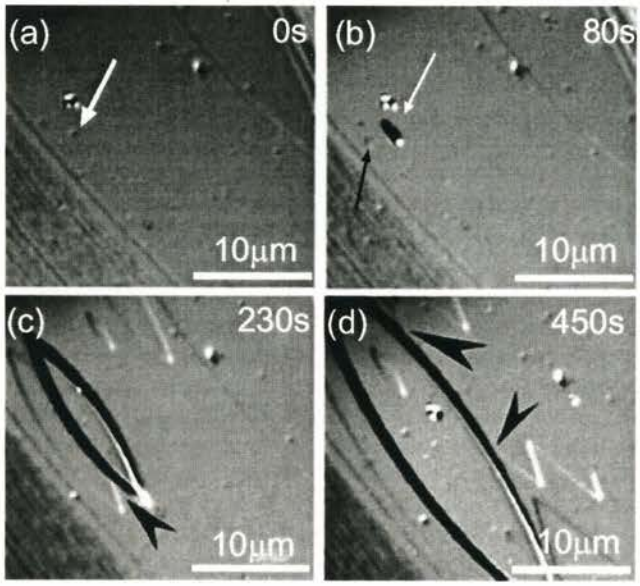


**Figure 8.** Micrographs of 2D nucleation and subsequent lateral growth of a multilayer island on a {110} face of a growing tetragonal lysozyme crystal, taken by LCM-DIM. The sequence of micrographs shows the time course of the multilayer island: 0 s (**a**), 80 s (**b**), 230 s (**c**), and 450 s (**d**). White arrows indicate the presence of foreign particles on the surface. The black arrow shows the nucleation of a 2D island with elementary step height. Black arrowheads indicate the positions at which the multilayer island overgrows the single-layered islands. Growth conditions: 38 mg/ml 99.99% pure lysozyme, 25 mg/ml NaCl, in 50 mM sodium actetate buffer (pH 4.5), and at 23.0℃. Reprinted with permission from the reference [49]. Copyright 2007 American Chemical Society.

## SINGLE-MOLECULE VISUALIZATION ON A PROTEIN CRYSTAL SURFACE

During crystal growth processes, the adsorption, surface diffusion and desorption of molecules are essential elementary processes, and hence have attracted attention over many years. In the field of surface physics, many scanning tunneling microscopy studies have been performed under ultra-high-vacuum conditions to clarify the adsorption, surface diffusion, and desorption behavior of individual adatoms and admolecules on a wide variety of crystal surfaces. In contrast, in the case of growth from a solution, no one has yet succeeded in observing mobile individual solute molecules at an interface between a solution and a crystal, although solution-crystal interfaces have many physicochemically important, but still unknown features, such as electric double layers, solvation, and desolvation. Our poor understanding of the dynamic behavior at a solution-crystal interface is due to the absence of studies on the noninvasive observation of solute molecules at this interface at the single-molecule level.

To achieve such visualization, we adopted a single-molecule visualization technique, which is a popular technique in the field of biological physics and enables us to visualize individual fluorescence-labeled molecules. We specifically labeled only the ε-amino group of the N-terminal of lysozyme with a fluorescent reagent, tetramethylrhodamine-5-isothiocyanate, in accordance with the recipe of Matsui *et al.* [62] Since the molecular weight of a fluorescent label after the reaction (tetramethylrhodamine) is less than 3% of that of fluorescence-labeled lysozyme (F-lysozyme), we expect that the fluorescent label will not exert a significant effect on the translational and rotational diffusion of F-lysozyme. In addition, most of the molecular surface of F-lysozyme is the same as that of native lysozyme, hence we also expect that the interaction between an F-lysozyme molecule and a lysozyme molecule aligned on a crystal surface will be almost the same as that in the case of a native lysozyme molecule on a crystal surface. This strong similarity between F-lysozyme and native lysozyme molecules allowed us to simulate the behavior of a solute molecule at a solution-crystal interface.

### Surface Diffusion on a Protein Crystal Surface

First we attempted to visualize the diffusion processes of individual F-lysozyme molecules at the interface of a solution and the {110} surface of a tetragonal lysozyme crystal [61]. (Fig. **9**) exhibits a typical single-molecule image: the right side of the image is a solution-crystal interface, and the left side corresponds to a bulk solution. Individual fluorescent spots (for example, the open circle in (Fig. **9**)) indicate individual F-lysozyme molecules. F-lysozyme molecules diffused at the solution-crystal interface but were not fixed on the crystal surface ((Fig. **9**) inset: the fluorescent spot appeared to be slightly elongated in the direction of motion of the molecule). In contrast, fluorescent spots were seldom observed in the bulk solution (discussed later in detail). The average number density of F-lysozyme molecules observed at the interface was $1.8 \times 10^{11}$ $m^{-2}$. From the fluorescence intensity and three-dimensional diffusion rate of F-lysozyme

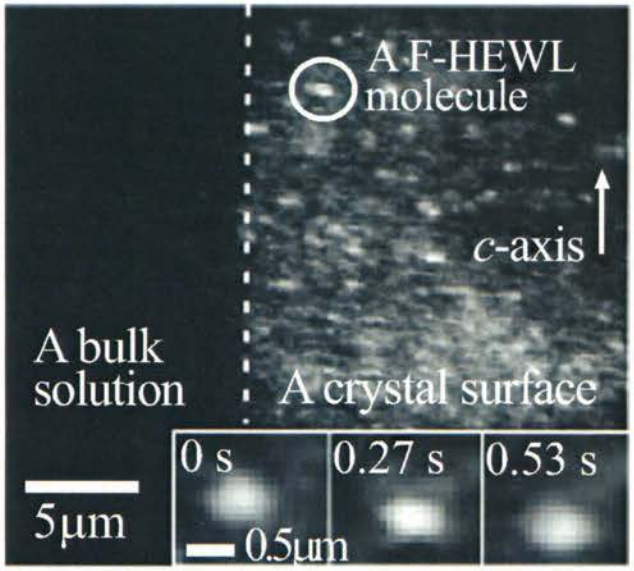


**Figure 9.** Typical single-molecule image from *in situ* observation. The right side shows a solution-crystal interface, and the left side shows a bulk solution. Fluorescent spots (open circle) indicate individual F-lysozyme molecules. The inset shows the time course of the movement of a F-lysozyme molecule. Reprinted with permission from the reference [61]. Copyright 2008 American Chemical Society.

molecules, we concluded that we cannot visualize F-lysozyme molecules diffusing in a bulk solution, i.e., the molecules observed in (Fig. **9**) strongly interacted with the crystal surface.

We determined the positions of F-lysozyme molecules using homemade software [74], which applied a Gaussian fitting algorithm [75] that estimated positions to a greater accuracy than one pixel size (87 nm). Irrespective of the elongation of a single-molecule spot (Fig. **9** inset), we could determine the position of the center of the spot by the Gaussian fitting algorithm. (Fig. **10a**) shows typical trajectories of F-lysozyme molecules at 33 ms intervals. The use of tetramethylrhodamine as a fluorescent label resulted in an accuracy of position determination of ±30 nm, which was estimated from the standard deviation of the positions of F-lysozyme molecules fixed on a glass plate. (Fig. **10a**) demonstrates that we could track the movements of individual F-lysozyme molecules with sufficient accuracy for subsequent analyses. All the crystal surfaces used in this study were covered with two-dimensional islands, and their average interstep distance was longer than 5 μm, which was significantly longer than the size of the area where the molecules diffused (Fig. **10a**). Hence, the diffusion observed in this study proceeded mainly on terraces.

(Fig. **10b**) presents typical changes in the mean square displacement $\langle d(n\Delta t)^2 \rangle$ in two dimensions as a function of time $n\Delta t$. All plots give the appearance that they follow straight lines, implying that their diffusion is close to simple random diffusion. Although some of the plots appear to deviate from the straight lines (e.g., 1 and 3 in (Fig. **10b**)), we could not find any clear correlation among the data measured

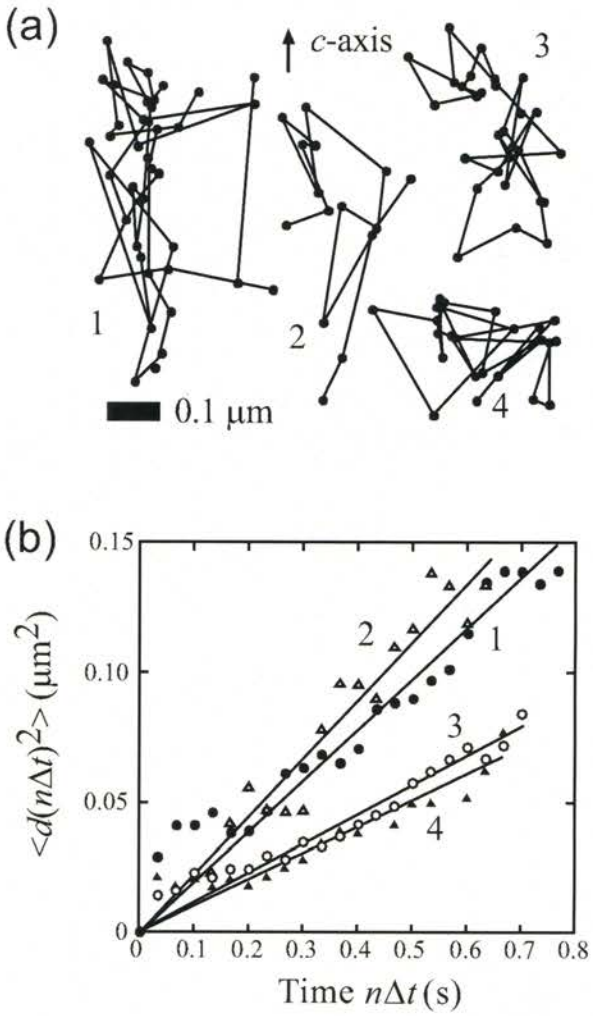


**Figure 10.** Diffusion of individual F-lysozyme molecules at a solution-crystal interface. (**a**) Typical trajectories of F-lysozyme molecules at 33 ms intervals. (**b**) Changes in the mean square displacement $\langle d(n\Delta t)^2 \rangle$ in two dimensions as a function of time $n\Delta t$. Numbers by the lines correspond to the molecules shown in (**a**). Reprinted with permission from the reference [61]. Copyright 2008 American Chemical Society.

for 293 F-lysozyme molecules. Hence, we carried out the following analyses assuming simple random diffusion.

We calculated the 2D diffusion coefficient $D$ from the average value of $\langle d(n\Delta t = 1\ \mathrm{s})^2 \rangle$ and the relation

$$\langle d(n\Delta t)^2 \rangle = 4D \cdot n\Delta t . \quad (2)$$

The 2D diffusion coefficient determined from 293 F-lysozyme molecules was $D$=(6.9 ± 1.2)x10$^{-15}$ m$^2$/s. It should be emphasized that the diffusion coefficient measured at the solution-crystal interface was 4-5 orders of magnitude smaller than that in the bulk solution (1.1×10$^{-10}$ m$^2$/s) [76]. We also experimentally determined the population distribution of the residence time of 293 F-lysozyme molecules at the solution-crystal interface. We found that the population is maximum at a residence time of 0.47 ± 0.08 s. The average

diffusion length of F-lysozyme molecules at the solution-crystal interface, evaluated from the residence time giving the maximum population, the value of $D$, and eq. (2), was 0.11 μm.

The result that the diffusion constant measured at the solution-crystal interface was 4-5 orders of magnitude smaller than that in the bulk solution clearly demonstrates that the F-lysozyme molecules visualized at the solution-crystal interface interacted strongly (mainly via hydrogen bonding) with the crystal surface, and diffused slowly in two dimensions within the range of hydrogen bonding (a distance up to about one nm), as schematically shown in (Fig. **11**). In (Fig. **9**), we also noted that the background fluorescence intensity at the solution-crystal interface was significantly higher than that in the bulk solution. This also clearly indicates strong interactions from the crystal surface. Compared with F-lysozyme molecules diffusing in a bulk solution, F-lysozyme molecules at the maximum distance at which hydrogen bonding could occur (Fig. **11**) interacted more strongly with the crystal surface, and hence the concentration of such molecules became higher. Therefore, we presume that such molecules appeared as the blurred area in the inset of (Fig. **11**). From the slow 2D diffusion and higher background intensity at the solution-crystal interface, we concluded that we observed the slow 2D diffusion of F-lysozyme molecules within the range of interactions from the crystal surface, although we could not completely eliminate the contribution of the bulk 3D diffusion because of the obscure border between the range of interactions and a bulk solution. The existence of a range of interactions in which solute molecules diffuse slowly is the largest difference from the case of diffusion at a vacuum-crystal interface. We emphasize that slow diffusion of solute molecules inside a thin 2D layer (Fig. **11**) presents the general picture of surface diffusion at an interface between an aqueous solution and a hydrophilic crystal surface, where electrostatic interactions play a key role.

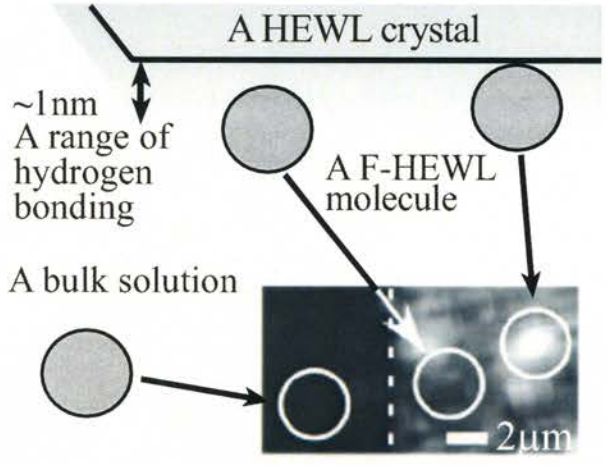


**Figure 11.** Schematic illustration of a cross-sectional view of a solution-crystal interface and F-lysozyme molecules diffusing in the vicinity of the interface. The inset shows a single-molecule image of F-lysozyme molecules. The layer of 1 nm thickness on the crystal surface represents the range of hydrogen bonding. Reprinted with permission from the reference [61]. Copyright 2008 American Chemical Society.

To demonstrate the condensation of F-lysozyme molecules at the solution-crystal interface, we measured the number density of F-lysozyme molecules at the interface. The average number density measured from single-molecule images was $1.8\mathbf{x}10^{11}$ $1/m^2$. In contrast, the number density of F-lysozyme molecules inside a layer of one molecule thickness (3.5 nm: evaluated from crystallographic data [77]), calculated from its bulk concentration (0.1 nM), was $2.1\mathbf{x}10^{8}$ $1/m^2$. Therefore, the surface concentration (number density) of F-lysozyme molecules became three orders of magnitude higher at the interface than in the bulk solution. We emphasize that such drastic condensation at the solution-crystal interface has been observed for the first time in this study, and has not yet been taken into account in existing theories of solution growth.

**Adsorption and Desorption on a Protein Crystal Surface**

We also attempted to visualize the transient processes during the adsorption of solute molecules onto a crystal surface [60]. We first investigated the adsorption sites of F-lysozyme molecules on the {110} face of a tetragonal lysozyme crystal. (Fig. **12a**) shows a typical single-molecule image: each bright dot corresponds to one F-lysozyme molecule adsorbed on a crystal surface. (Fig. **12b**) represents the same field of view observed by LCM-DIM. In (Fig. **12b**), a white arrow shows the position where steps with stronger contrast, probably corresponding to bunched steps, were observed on the crystal surface. A comparison of images a and b clearly demonstrates that F-lysozyme molecules were preferentially adsorbed on steps (not on terraces). This result suggests that the F-lysozyme molecules behaved as native lysozyme molecules during the adsorption onto a lysozyme crystal surface, unaffected by the presence of a low-molecular-weight fluorescent label (<3% of the molecular weight of F-lysozyme).

To distinguish the molecules immobilized on a crystal surface from those diffusing on the surface, we compared the positions of the molecules recorded in a series of time frames. Under our experimental conditions, each fluorescent spot exhibits a Gaussian distribution of several pixels to 6 pixels in diameter (inset of (Fig. **13c**)). When the center positions of spots in time frames were matched within one pixel size (87 nm), we judged that such molecules did not change their positions during that time interval. (Figs. **13a** and **b**) present examples of single-molecule images with a 1 s time interval. In (Fig. **13a**), circles correspond to all F-lysozyme molecules visualized at the interface. In (Fig. **13b**), circles indicate the molecules whose positions did not change during 1 s, i.e., the molecules immobilized on the crystal surface for at least 1 s. Hereafter, we define the molecules that were immobilized on the crystal surface, as "adsorbed" molecules; in this case, the use of this word does not include molecules diffusing on the crystal surface.

Because of the sufficiently dilute concentration of F-lysozyme in the solution (0.1 nM) and the very short surface diffusion length (0.11 μm), we concluded that we can reject the case in which one molecule is desorbed and a second molecule is adsorbed at the same location. Hereafter, we define the time interval during which the molecule did not change its position on the crystal surface as the residence time $\tau$.

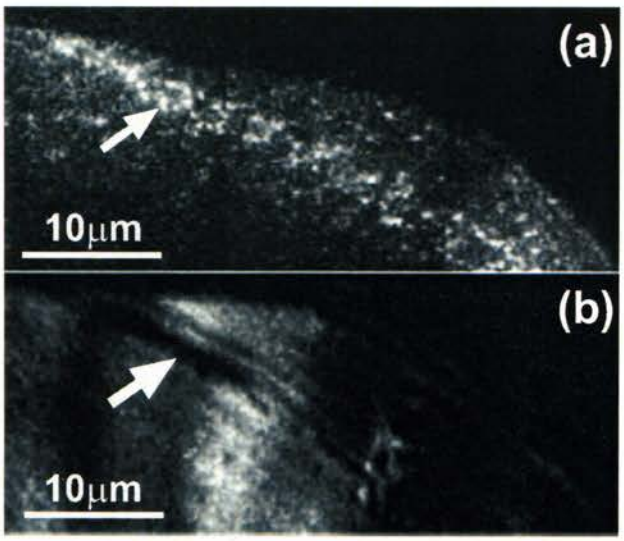


**Figure 12.** Images taken by single-molecule visualization of an oblique illumination type (**a**) and by LCM-DIM (b). The same field of view on the {110} face of a tetragonal lysozyme crystal was observed by both methods 116 min after F-lysozyme molecules were introduced into an observation chamber. (**a**) Each bright dot corresponds to one F-lysozyme molecule adsorbed on the crystal surface. The image was composed of three frame images because of the limited field of view of the EM-CCD camera. In (**b**), the arrow shows the position where steps with a stronger contrast level can be observed, probably corresponding to bunched steps. Reprinted with permission from the reference [60]. Copyright 2011 American Chemical Society.

(Fig. **13c**) is an image taken 300 s after the image in (Fig. **13a**). The circles in (Fig. **13c**) indicate molecules that did not move between the images in (Figs. **13a** and **c**) and therefore have $\tau \geq 300$ s. Note that the number of molecules with $\tau \geq 300$ s is significantly smaller than that with $\tau \geq 1$ s (Fig. **13b**), indicating significant desorption of the molecules during this period. Most of the molecules shown in (Fig. **13c**) (not marked by circles) appeared on the crystal surface after (Fig. **13a**) was taken.

We observed the movement of F-lysozyme molecules using discontinuous pulsed laser illumination following the procedure shown in (Fig. **13d**). At a given elapsed time after the introduction of F-lysozyme molecules into the observation chamber, $t_{ads}$, we determined the number density $N$ of molecules whose positions had not changed during a series of residence times $\tau$. Hence, the number density $N(t_{ads}, \geq\tau)$ does not include molecules that were newly adsorbed during time $\tau$ after $t_{ads}$.

We obtained systematic changes in $N(t_{ads}, \geq\tau)$ for various $\tau$ as a function of $t_{ads}$ (Fig. **14**). We found an induction period (~70 min) before the sudden increase in $N(t_{ads}, \geq\tau)$. After the induction period, $N(t_{ads}, \geq\tau)$ increased linearly with adsorption time. The dashed lines after the induction period in (Fig. **14**) show the results of linear fitting. Our results are considerably different from those of previous conventional adsorption studies [78-80], in which no induction period was observed ($N$ started to increase from $t_{ads} = 0$). The existence of the induction period indicates that the adsorption did not proceed through a single-step adsorption process. If a single-step adsorption process occurred, the probability that an in-

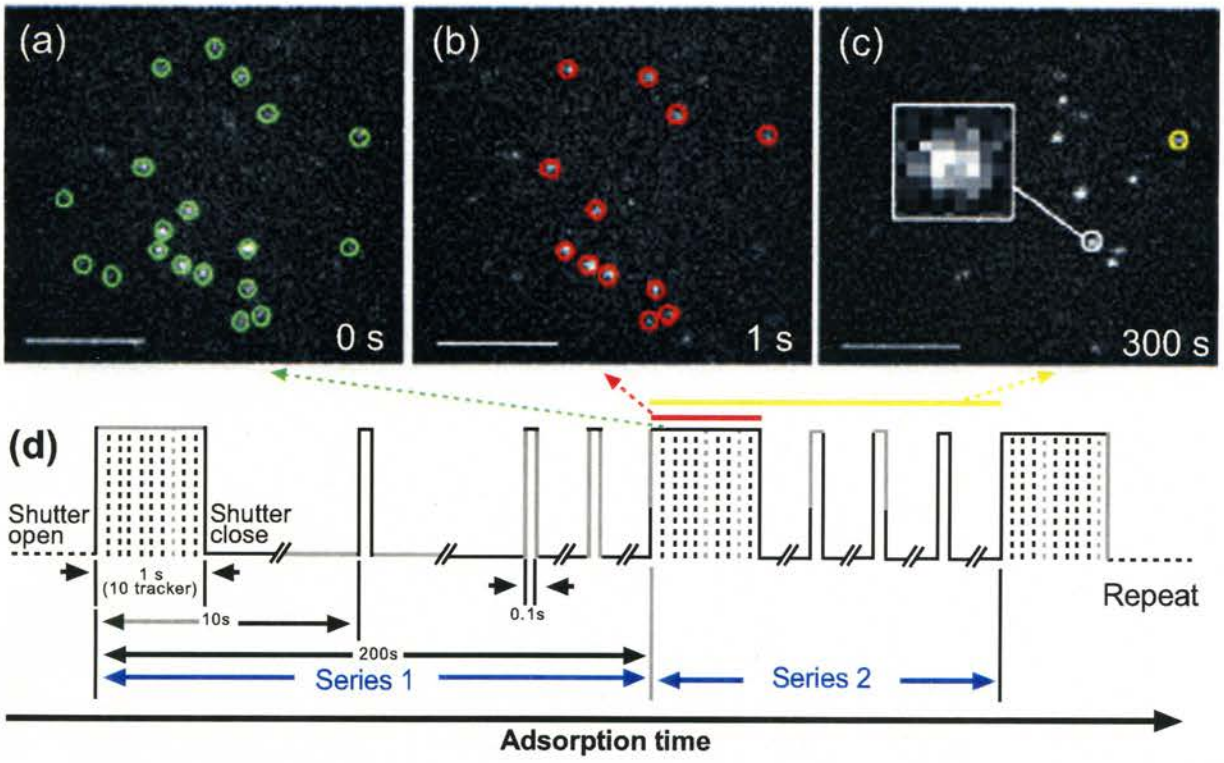


**Figure 13.** Nonensemble measurements of transient processes of adsorption on a lysozyme crystal surface. (**a**)-(**c**) Typical time course of F-lysozyme molecules appearing on the crystal surface taken 61 min after the molecules were introduced into the observation chamber. Scale bars represent 5 μm. (**a**) Circles show all the F-lysozyme molecules visualized on the crystal surface. (**b**) and (**c**) Circles correspond to molecules whose positions did not change for periods longer than 1 and 300 s, respectively. (**d**) Time-sequence diagram of discontinuous pulsed laser illumination. Reprinted with permission from the reference [60]. Copyright 2011 American Chemical Society.

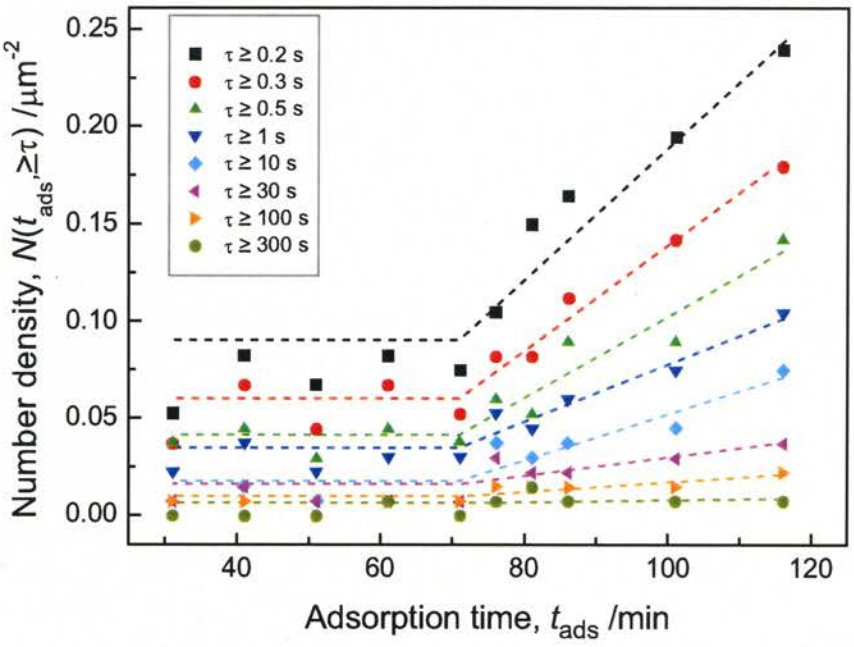


**Figure 14.** Changes in number density $N(t_{ads}, \geq\tau)$ of F-lysozyme molecules with unchanged positions, within an accuracy of one pixel size, for longer than the residence time $\tau$, as a function of adsorption time $t_{ads}$. The residence time $\tau$ was varied from 0.2 to 300 s. The total irradiation time of the crystal surface with the discontinuous pulsed laser illumination was 31 s, and the step density of the observed crystal surface was 0.12 μm$^{-1}$. Reprinted with permission from the reference [60]. Copyright 2011 American Chemical Society.

dividual molecule overcame the activation energy barrier to the process would be proportional to the number of attempts, i.e., to the elapsed time, $t_{ads}$. Therefore, the results shown in (Fig. **14**) suggest that the adsorption proceeded through a series of successive multistep processes. We consider that dehydration of protein molecules is a likely cause for the series of successive multistep processes occurring during adsorption, although we do not have any experimental evidence for this hypothesis.

Furthermore, (Fig. **14**) shows that with increasing $\tau$ at the same $t_{ads}$, $N(t_{ads}, \geq\tau)$ becomes significantly smaller. This result clearly demonstrates that stronger adsorption with a longer $\tau$ is less likely than weaker adsorption with a shorter $\tau$, implying that the adsorption of molecules onto the crystal surface becomes gradually stronger over a number of trials. The gradual immobilization of solute molecules on the crystal surface corresponds to the gradual change in the order parameter during the transition from solute to solid states.

## OBSERVATION OF IMPURITY EFFECTS BY LCM-DIM AND SINGLE-MOLECULE VISUALIZATION

Generally, impurities are considered to affect the growth process after they are adsorbed on a crystal surface. Thus, to fully comprehend the mechanisms of impurity effects, one must observe, *in situ*, both 1) the dynamics of elementary steps and 2) the adsorption of impure molecules on the crystal surface, at the molecular level. In this study, we used LCM-DIM and single-molecule visualization of an oblique illumination type, and simultaneously observed elementary growth steps and fluorescence-labeled protein molecules on the {110} faces of tetragonal crystals [48].

As protein impurities, we used F-lysozyme, dimer of lysozyme, and 18kDa protein (the last two are major impurities of the Seikagaku lysozyme) [81]. We also used F-lysozyme and fluorescence-labeled dimer of lysozyme (F-dimer) to observe the adsorption sites of these proteins on a crystal surface. From these *in situ* observations, we attempted to directly clarify the relationship between the adsorption sites of impurities on a crystal surface and the effects of the protein impurities on the advancement of elementary steps.

Before showing the details of experiments and their results, we supplement the effects of the fluorescence label of F-lysozyme. For the surface diffusion, adsorption and desorption processes of F-lysozyme molecules on a crystal surface, we can expect that the fluorescence label does not give significant effects. In contrast, F-lysozyme molecules effectively suppress the growth of tetragonal lysozyme crystals as impurity [62], since the fluorescence label is located at a molecular surface of lysozyme inside of the intermolecular contact area in a tetragonal crystal. Then once an F-lysozyme molecule becomes adsorbed on a tetragonal-crystal surface, the fluorescent label blocks the formation of subsequent intermolecular contact, causing significant impurity effects.

We measured step velocities of 2D islands in the long-axis direction, since the growth in the long-axis direction is more affected by impurities than that in the short-axis direction [50]. Then to evaluate the effects of these protein impurities quantitatively, we calculated the ratios $R$ of the step velocity in the 99.99% pure lysozyme solution, $v_{99.99\%\ \text{purity}}$, to the step velocities in the solutions containing impurities, $v_{\text{F-lysozyme}}$, $v_{\text{dimer}}$, $v_{18\text{kDa}}$, and $v_{98.5\%\ \text{purity}}$, at the same supersaturation. Thus, the ratio $R$ corresponds to the amount of suppression of the step velocity by impurities compared with that in the case of the 99.99% pure solution.

To calculate the ratio $R$, we fitted all the experimental data ($v$ vs $C$-$C_e$ plots) with a local polynomial regression (LOESS) [82, 83]. Using the values obtained from the LOESS fits, we calculated the ratio $R$ at the same supersaturation (Fig. **15**). Since, in the curve fitting, the typical error in the step velocity measurement at a given supersaturation was about 1% for 99.99% pure lysozyme solutions and 3% for Seikagaku lysozyme solutions, the step velocity measurement was sufficiently accurate. Hence, the error in the ratio $R$ mainly originated from the local polynomial regression. The error bars shown in (Fig. **15**) were calculated from the standard error (90% statistical significance) of our fitting model and the propagation of errors.

As shown in (Fig. **15**), the value of $R$ increased with increasing impurity concentration for all three protein impurities, showing the stronger suppression of the step velocity with increasing impurity concentration. However, the different protein impurities have different $R$ values and also show different supersaturation dependences of $R$. Taking into account the large error of the ratio $R$ in the low supersaturation range (in particular, $C$-$C_e$<10 mg/ml), the differences in the values and shapes of the $R$ vs supersaturation plots are still significant. For the same impurity, the shape of the $R$ vs supersaturation plot does not change regardless of the impurity concentration.

As shown in (Fig. **12**), F-lysozyme was preferentially adsorbed on steps (more precisely, kinks). Then we also observed the adsorption sites of the F-dimer on the {110} face of a tetragonal lysozyme crystal. (Fig. **16a**) shows a typical single-molecule image; each bright dot corresponds, in principle, to one F-dimer molecule adsorbed on the crystal surface. (Fig. **16b**) indicates the same field of view as that observed by LCM-DIM. The arrows show the positions of bunched steps on the crystal surface, and an arrowhead indicates the position of an elementary step. A comparison of (Figs. **16a** and **b**) clearly indicates that F-dimer molecules are adsorbed randomly on terraces of the {110} face, in contrast to the case of F-lysozyme. The results shown in (Figs. **12** and **16**) experimentally suggest that a microheterogeneous protein impurity molecule, for which the intermolecular bonding to the crystal surface is similar to that of a solute molecule, is preferentially adsorbed on a step (i.e., kink), and that a microheterogeneous protein impurity molecule with different intermolecular bonding from that of a solute mole-

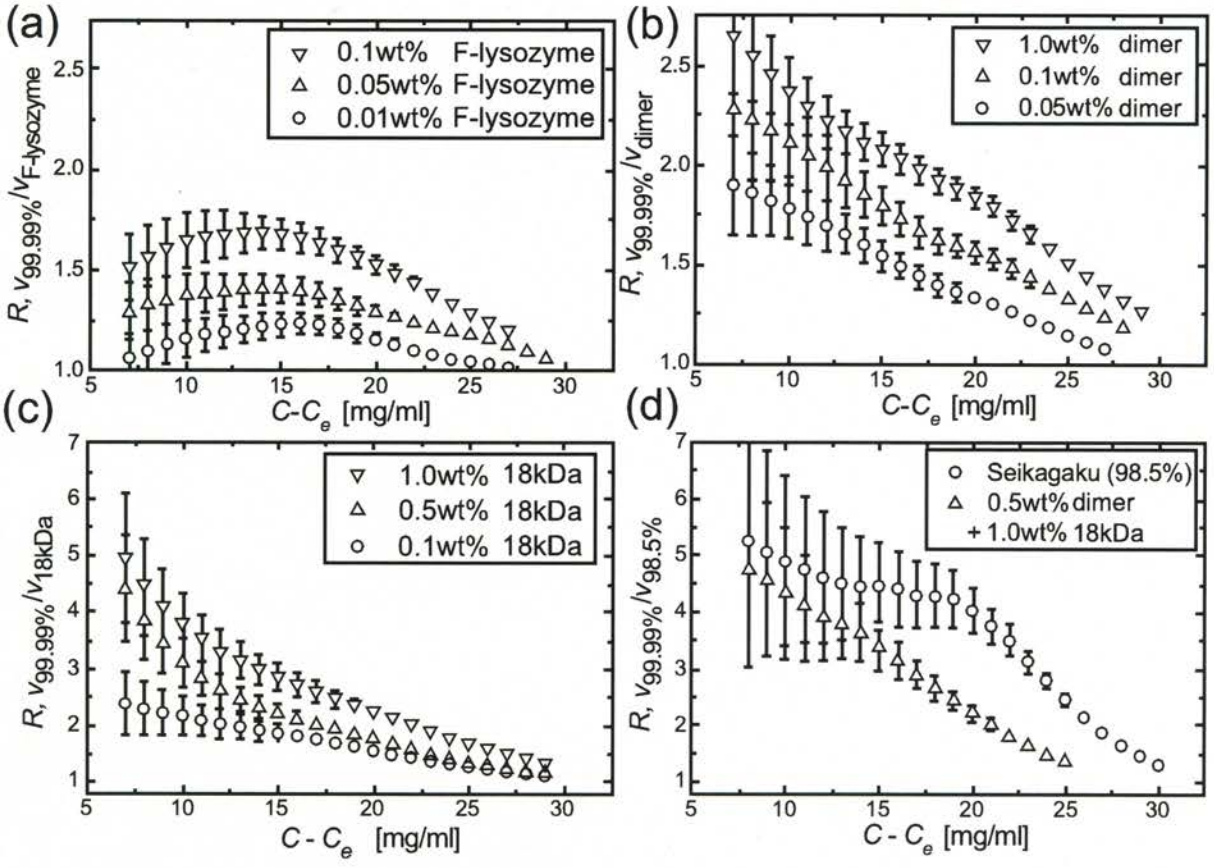


**Figure 15.** Changes in the ratios $R$ of the step velocity in a 99.99% pure solution, $v_{99.99\%\ \text{purity}}$, to those in solutions containing impurities, $v_{\text{F-lysozyme}}$, $v_{\text{dimer}}$, $v_{\text{dimer}}$, and $v_{98.5\%\ \text{purity}}$, as a function of supersaturation. $R$ was calculated from the fitted curves of $v$ vs $C$-$C_e$ plots. Here $C$ is the solute concentration and $C_e$ the solubility. The errors were evaluated from the standard error (90% statistical significance) and the propagation of errors. All crystals were grown from 99.99% pure lysozyme solutions with a concentration of 40 mg/ml. Protein impurities added intentionally: (**a**) 0.01-0.1 wt% F-lysozyme, (**b**) 0.05-1.0 wt% dimer, (**c**) 0.1-1.0 wt% 18kDa protein molecules, and (**d**) 0.5 wt% dimer and 1.0 wt% 18kDa protein molecules. In (**d**), the results for Seikagaku lysozyme (98.5% purity) solutions of 40 mg/ml are also plotted. Other growth conditions: 25 mg/ml NaCl, in 50 mM sodium acetate (pH 4.5), and at 18.0-26.0°C. Reprinted with permission from the reference [48]. Copyright 2009 American Chemical Society.

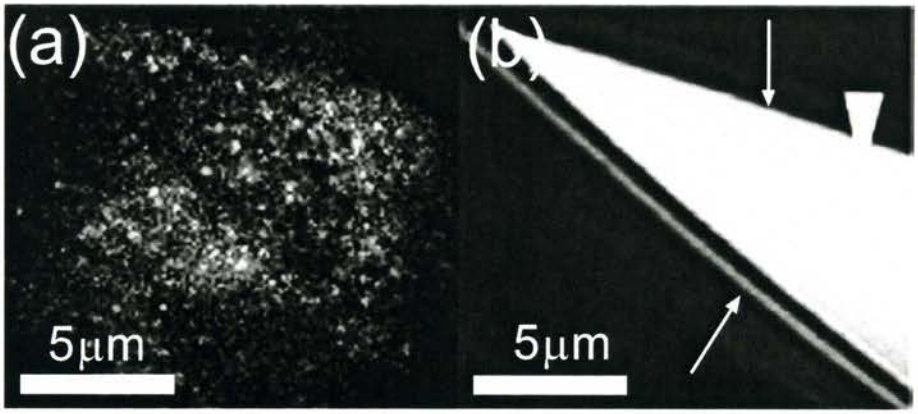


**Figure 16.** Adsorption sites of F-dimer on {110} surface of tetragonal lysozyme crystal. The same field of view was observed by single-molecule visualization of an oblique illumination type (**a**) and by LCM-DIM (**b**). (**a**) Each bright dot corresponds to one F-dimer molecule adsorbed on the crystal surface. (**b**) Arrows show the positions of bunched steps on the crystal surface, and an arrowhead indicates the position of an elementary step. Conditions: 99.99% pure lysozyme solution of 27 mg/ml, 0.1 nM F-dimer, 25 mg/ml NaCl, in 50 mM sodium acetate (pH 4.5), and at 24.0°C. Reprinted with permission from the reference [48]. Copyright 2009 American Chemical Society.

cule is preferentially adsorbed on different sites of the crystal surface.

From the difference in the adsorption sites of F-lysozyme and F-dimer, we attempted to explain the different dependences of the ratio $R$ on supersaturation shown in (Fig. **15**). Impurity models can be essentially divided into two groups. (I) The adsorption of impurity molecules at kink sites leading to kink blocking; this was first proposed by Bliznakov [84], and presented more extensively by Chernov [71]. (II) The adsorption of impurity molecules on terraces (or steps) leading to step pinning, which was first described in the pioneering work of Cabrera and Vermileya [85]. A more exhaustive overview of impurity models can be found in the work of Sangwal [86]. We attempted to explain our observations by taking into account these two impurity models.

For F-lysozyme, steps (more precisely, kinks on steps) are the major adsorption sites. The movement of a growth ledge (i.e., step) is simultaneously caused by the different rates of attachment of growth entities at incorporation sites (kinks) occupied and unoccupied with impurities [87]. Under a low supersaturation range, F-lysozyme molecules have sufficient time for adsorption because of the slow advancement of steps. Hence, in this supersaturation range, it is reasonable to assume that the adsorption and desorption of F-lysozyme molecules on a step (i.e., kinks) reach equilibrium: i.e., the ratio of the number of kinks occupied by impurities to the total number of kinks on a step becomes constant irrespective of supersaturation [88], as schematically shown in (Fig. **17a**). Under a low supersaturation range, since the ratio of the number of kinks occupied by impurities to the total number of kinks on a step is constant, the $v$ vs $C$-$Ce$ plot follows a line (labeled "impure" in (Fig. **17b**)) with a constant slope and a kinetic coefficient smaller than that in the case of a pure sample.

With increasing supersaturation, the increase in step velocity decreases the exposure time of adsorption sites to impurities in a solution [88], and this tends to decrease the impurity effects (i.e., fewer kink sites are blocked by impurity molecules). Hence in an intermediate supersaturation range, with increasing supersaturation, the ratio of the number of kinks occupied by impurities to the total number of kinks on a step decreases and finally reaches zero under a high supersaturation range (Fig. **17a**). Therefore, under a high supersaturation range, the $v$ vs $C$-$Ce$ plot follows the line that is observed in the case of the pure sample (labeled "pure" in (Fig. **17b**)). Under an intermediate supersaturation range, the transition of the $v$ vs $C$-$Ce$ plot from the impure line to the pure line is observed. According to such a picture, the phenomena that we observed can be explained as follows (Fig. **17c**). Under a low supersaturation range, the degree of the impurity effect (the ratio $R$) remains constant with increasing supersaturation, and in the middle and high supersaturation ranges, $R$ decreases with increasing supersaturation.

In the case of the dimer, terraces are the major adsorption sites on the {110} faces (Fig. **16**). Thus, to describe the impurity effects of the dimer on step advancement, we follow the step-pinning model [85], in which the impurity effect is analyzed by comparing the critical curvature of a step to the average spacing of adsorbed impurities.

Under a low supersaturation range, dimmers show equilibrium adsorption on a terrace, as schematically shown in (Fig. **18a**). In (Fig. **15b**), we did not observe a plateau under a low supersaturation range, where $R$ remained constant. This result can be satisfactorily explained by taking into account the supersaturation dependence of the radius of the critical nucleus. Assuming a circular 2D nucleus, its critical radius $\rho_{crit.}$ is inversely proportional to $\Delta\mu$, where $\Delta\mu$ is the chemical potential difference between molecules in a crystal and a solution. Hence, with increasing supersaturation, $\rho_{crit.}$ decreases (Fig. **18b**). On the other hand, the distance $d$ between adjacent dimer molecules adsorbed on a terrace can be expressed as $d = 1/\sqrt{N_{2D}}$, where $N_{2D}$ is the number of dimer molecules adsorbed per unit area. When $d < 2\rho_{crit.}$, steps stop advancing (supersaturation range I in (Fig. **18b**): in this region, $R$ cannot be defined. However in supersaturation range II (Fig. **18b**), where the equilibrium adsorption of the dimer still exists, with increasing super-

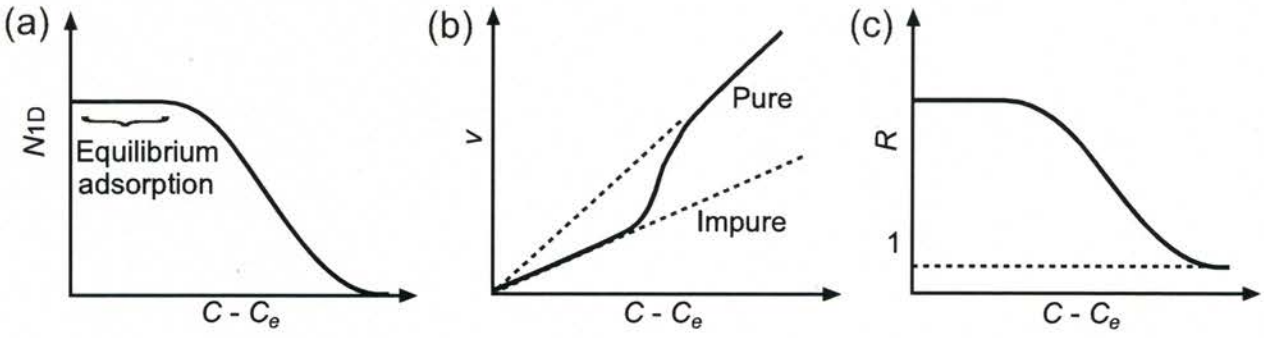


**Figure 17.** Schematic illustrations of impurity effects of F-lysozyme. Supersaturation dependences of number density $N_{1D}$ [1/m] of adsorbed F-lysozyme on a step (**a**), step velocity $v$ (**b**), and ratio $R$ (**c**). Using $\lambda_0$ (average distance between kinks) and $\lambda_i$ (average distance between free kinks), $N_{1D}$ is expressed as $N_{1D} = 1/\lambda_0 - 1/\lambda_i$ ($0 \le N_{1D} \le 1/\lambda_0$). Reprinted with permission from the reference [48]. Copyright 2009 American Chemical Society.

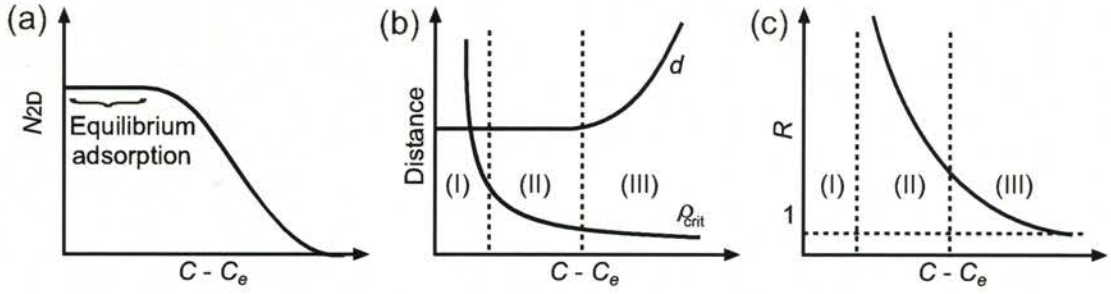


**Figure 18.** Schematic illustrations of impurity effects of dimer. Supersaturation dependences of number density $N_{2D}$ [1/m$^2$] of adsorbed dimer on a terrace (**a**), $d$ (distance between adjacent dimer molecules adsorbed on a terrace) and $\rho_{crit.}$ (radius of a critical 2D nucleus) (**b**), and ratio $R$ (**c**). Here, $d$ is calculated as $d = 1/\sqrt{N_{2D}}$. Reprinted with permission from the reference [48]. Copyright 2009 American Chemical Society.

saturation, a decrease in $\rho_{crit.}$ results in a decrease in the impurity effect (i.e., $R$). In supersaturation range III, the decrease in $\rho_{crit.}$ and the increase in $d$ decrease the impurity effect with increasing supersaturation. The supersaturation range observed in (Fig. **15b**) corresponds to the ranges II and III in (Fig. **18c**).

For the 18kDa impurity protein, we observed a very similar dependence of $R$ on supersaturation to that observed for the dimer (Figs. **15b** and **c**). Taking into account the fact that the intermolecular bonding between a 18 kDa molecule and a crystal surface is different from that in the case of a native lysozyme molecule, it seems reasonable to assume that 18 kDa molecules are also adsorbed randomly on terraces, as in the case of the dimer.

The impurity effects observed for Seikagaku lysozyme were more complex (Fig. **15d**), and could not be reproduced using the solution containing 0.5 wt% dimer and 1.0 wt% 18 kDa molecules, although these are the main impurities included in Seikagaku lysozyme [81]. This result indicates that trace amounts of other impure molecules present in Seikagaku lysozyme play a significant role in exhibiting the impurity effect.

## CONCLUSION

In this review, we demonstrated that the visualization of elementary steps and single protein molecules on protein crystal surfaces is a powerful means of studying the elementary growth processes of protein crystals. Utilizing this means, research in the field of crystal growth should move toward clarifying the mechanisms of defect generation in protein crystals. In addition, as described in the introduction, it is necessary to investigate the correlation between lattice defects and the diffraction properties of protein crystals. To achieve this, close collaboration between the fields of crystal growth and structural biology will be indispensable.

Finally, we remark on another direction of future research. Since protein molecules are much larger than inorganic salts and low-molecular-weight compounds, *in situ* observation of their elementary growth processes is much easier. Hence, utilizing the similarities between the growth mechanisms of protein crystals and inorganic/low-molecular-weight-compound crystals, protein crystals may become a promising model system for elucidating many physicochemically important but still unknown phenomena occurring at solution-crystal interfaces, such as electric double layers, solvation, and desolvation.

## ACKNOWLEDGEMENTS

The authors thank Y. Saito and S. Kobayashi (Olympus Engineering Co., Ltd.) for their technical support in the development of LCM-DIM, and H. Higuchi (The University of Tokyo) and T. Watanabe (Osaka University) for their technical assistance and valuable discussion on single-molecule

visualization experiments. This work was partially supported by Grants-in-Aid Nos. 16360001, 17034007, and 18360003 for Scientific Research from the Ministry of Education, Science and Culture of Japan (G.S.) and Project Research B at the Center for Interdisciplinary Research, Tohoku University (G.S. and G.D.), Grant No. AYA2009-10655 from the Ministry of Science and Innovation, Spain (F.O, and A.V.D), and the Consolider-Ingenio 2010 project "Factoría Española de cristalización" (F.O, and A.V.D).

## REFERENCES

[1] Durbin, S.D.; Carlson, W.E. Lysozyme Crystal-Growth Studied by Atomic Force Microscopy. *J. Cryst. Growth,* **1992**, *122*, 71-79.

[2] Durbin, S.D.; Feher, G. Studies of Crystal-Growth Mechanisms of Proteins by Electron-Microscopy. *J. Mol. Biol.,* **1990**, *212*, 763-774.

[3] Vekilov, P.G.; Ataka, M.; Katsura, T. Laser Michelson Interferometry Investigation of Protein Crystal-Growth. *J. Cryst. Growth,* **1993**, *130*, 317-320.

[4] Land, T.A.; Malkin, A.J.; Kuznetsov, Y.G.; McPherson, A.; Deyoreo, J.J. Mechanisms of Protein Crystal-Growth - an Atomic-Force Microscopy Study of Canavalin Crystallization. *Phys. Rev. Lett.,* **1995**, *75*, 2774-2777.

[5] Malkin, A.J.; Kuznetsov, Y.G.; Land, T.A.; Deyoreo, J.J.; McPherson, A. Mechanisms of Growth for Protein and Virus Crystals. *Nat. Struct. Biol.,* **1995**, *2*, 956-959.

[6] Durbin, S.D.; Feher, G. Protein crystallization. *Annu. Rev. Phys. Chem.,* **1996**, *47*, 171-204.

[7] Vekilov, P.G.; Monaco, L.A.; Rosenberger, F. Facet Morphology Response to Nonuniformities in Nutrient and Impurity Supply .1. Experiments and Interpretation. *J. Cryst. Growth,* **1995**, *156*, 267-278.

[8] Lin, H.; Vekilov, P.G.; Rosenberger, F. Facet morphology response to nonuniformities in nutrient and impurity supply .2. Numerical simulations. *J. Cryst. Growth,* **1996**, *158*, 552-559.

[9] Kurihara, K.; Miyashita, S.; Sazaki, G.; Nakada, T.; Suzuki, Y.; Komatsu, H. Interferometric study on the crystal growth of tetragonal lysozyme crystal. *J. Cryst. Growth,* **1996**, *166*, 904-908.

[10] Sazaki, G.; Kurihara, K.; Nakada, T.; Miyashita, S.; Komatsu, H., A novel approach to the solubility measurement of protein crystals by two-beam interferometry. *J. Cryst. Growth,* **1996**, *169*, 355-360.

[11] Rosenberger, F.; Lin, H.; Vekilov, P.G. Finite-amplitude instability in growth step trains with overlapping step supply fields. *Phys. Rev. E,* **1999**, *59*, 3155-3164.

[12] Vekilov, P.G.; Rosenberger, F.; Lin, H.; Thomas, B.R. Nonlinear dynamics of layer growth and consequences for protein crystal perfection. *J. Cryst. Growth,* **1999**, *196*, 261-275.

[13] Ramachandran, N.; Baugher, C.R.; Naumann, R.J. Modeling flows and transport in protein crystal growth. *Microgravity Sci. Technol.,* **1995**, *8*, 170-179.

[14] Savino, R.; Monti, R. Buoyancy and surface-tension-driven convection in hanging-drop protein crystallizer. *J. Cryst. Growth,* **1996**, *165*, 308-318.

[15] Pusey, M.; Naumann, R. Growth-Kinetics of Tetragonal Lysozyme Crystals. *J. Cryst. Growth,* **1986**, *76*, 593-599.

[16] Pusey, M.; Witherow, W.; Naumann, R. Preliminary Investigations into Solutal Flow About Growing Tetragonal Lysozyme Crystals. *J. Cryst. Growth,* **1988**, *90*, 105-111.

[17] Grant, M.L.; Saville, D.A. Long-Term Studies on Tetragonal Lysozyme Crystals Grown in Quiescent and Forced-Convection Environments. *J. Cryst. Growth,* **1995**, *153*, 42-54.

[18] Lin, H.; Rosenberger, F.; Alexander, J.I.D.; Nadarajah, A. Convective-Diffusive Transport in Protein Crystal-Growth. *J. Cryst. Growth,* **1995**, *151*, 153-162.

[19] Vekilov, P.G.; Lin, H.; Rosenberger, F. Unsteady crystal growth due to step-bunch cascading. *Phys. Rev. E,* **1997**, *55*, 3202-3214.

[20] Delucas, L.J.; Smith, C.D.; Smith, H.W.; Vijaykumar, S.; Senadhi, S.E.; Ealick, S.E.; Carter, D.C.; Snyder, R.S.; Weber, P.C.; Salemme, F.R.; Ohlendorf, D.H.; Einspahr, H.M.; Clancy, L.L.; Navia, M.A.; McKeever, B.M.; Nagabhushan, T.L.; Nelson, G.; McPherson, A.; Koszelak, S.; Taylor, G.; Stammers, D.; Powell, K.; Darby, G.; Bugg, C. E. Protein Crystal-Growth in Microgravity. *Science,* **1989**, *246*, 651-654.

[21] Delucas, L.J.; Smith, C.D.; Carter, D.C.; Snyder, R.S.; McPherson, A.; Koszelak, S.; Bugg, C.E. Microgravity Protein Crystal-Growth - Results and Hardware Development. *J. Cryst. Growth,* **1991**, *109*, 12-16.

[22] DeLucas, L.J. International Space Station. *Acta Astronaut.,* **1996**, *38*, 613-619.

[23] Carter, D.C.; Lim, K.; Ho, J.X.; Wright, B.S.; Twigg, P.D.; Miller, T.Y.; Chapman, J.; Keeling, K.; Ruble, J.; Vekilov, P.G.; Thomas, B.R.; Rosenberger, F.; Chernov, A.A. Lower dimer impurity incorporation may result in higher perfection of HEWL crystals grown in microgravity - A case study. *J. Cryst. Growth,* **1999**, *196*, 623-637.

[24] DeLucas, L.J.; Moore, K.M.; Long, M.M.; Rouleau, R.; Bray, T.; Crysel, W.; Weise, L. Protein crystal growth in space, past and future. *J. Cryst. Growth,* **2002**, *237*, 1646-1650.

[25] Garciaruiz, J.M.; Moreno, A.; Viedma, C.; Coll, M. Crystal Quality of Lysozyme Single-Crystals Grown by the Gel Acupuncture Method. *Mater. Res. Bull.,* **1993**, *28*, 541-546.

[26] Garcia-Ruiz, J.M.; Novella, M.L.; Otalora, F. Supersaturation patterns in counter-diffusion crystallisation methods followed by Mach-Zehnder interferometry. *J. Cryst. Growth,* **1999**, *196*, 703-710.

[27] Chernov, A.A.; Garcia-Ruiz, J.M.; Thomas, B.R. Visualization of the impurity depletion zone surrounding apoferritin crystals growing in gel with holoferritin dimer impurity. *J. Cryst. Growth,* **2001**, *232*, 184-187.

[28] Garcia-Ruiz, J.M.; Novella, M.L.; Moreno, R.; Gavira, J.A. Agarose as crystallization media for proteins I: Transport processes. *J. Cryst. Growth,* **2001**, *232*, 165-172.

[29] Garcia-Ruiz, J.M.; Otalora, F.; Novella, M.L.; Gavira, J.A.; Sauter, C.; Vidal, O. A supersaturation wave of protein crystallization. *J. Cryst. Growth,* **2001**, *232*, 149-155.

[30] Komatsu, H.; Miyashita, S.; Suzuki, Y. Interferometric Observation of the Interfacial Concentration Gradient Layers around a Lysozyme Crystal. *Jpn. J. Appl. Phys. Part 2-Letters,* **1993**, *32*, L1855-L1857.

[31] Miyashita, S.; Komatsu, H.; Suzuki, Y.; Nakada, T. Observation of the Concentration Distribution around a Growing Lysozyme Crystal. *J. Cryst. Growth,* **1994**, *141*, 419-424.

[32] Kuznetsov, Y.G.; Malkin, A.J.; Greenwood, A.; McPherson, A. Interferometric Studies of Growth-Kinetics and Surface-Morphology in Macromolecular Crystal-Growth - Canavalin, Thaumatin, and Turnip Yellow Mosaic-Virus. *J. Struct. Biol.,* **1995**, *114*, 184-196.

[33] Vekilov, P.G.; Monaco, L.A.; Rosenberger, F. High-Resolution Interferometric-Technique for in-Situ Studies of Crystal-Growth Morphologies and Kinetics. *J. Cryst. Growth,* **1995**, *148*, 289-296.

[34] Kashimoto, E.; Sazaki, G.; Hasegawa, K.; Nakada, T.; Miyashita, S.; Komatsu, H.; Sato, K.; Matsuura, Y.; Tanaka, H. Crystallization studies on a concanavalin A crystal with high-index faces. *J. Cryst. Growth,* **1998**, *186*, 461-470.

[35] Suzuki, Y.; Sazaki, G.; Matsui, T.; Nakajima, K.; Tamura, K. High-pressure acceleration of the growth kinetics of glucose isomerase crystals. *J. Phys. Chem. B,* **2005**, *109*, 3222-3226.

[36] Durbin, S.D.; Carlson, W.E.; Saros, M.T. In-Situ Studies of Protein Crystal-Growth by Atomic-Force Microscopy. *J. Phys. D Appl. Phys.,* **1993**, *26*, B128-B132.

[37] McPherson, A.; Malkin, A.J.; Kuznetsov, Y.G. The Science of Macromolecular Crystallization. *Structure,* **1995**, *3*, 759-768.

[38] Kuznetsov, Y.G.; Malkin, A.J.; Glantz, W.; McPherson, A. In situ atomic force microscopy studies of protein and virus crystal growth mechanisms. *J. Cryst. Growth,* **1996**, *168*, 63-73.

[39] Yau, S.T.; Vekilov, P.G. Quasi-planar nucleus structure in apoferritin crystallization. *Nature,* **2000**, *406*, 494-497.

[40] Galkin, O.; Vekilov, P.G. Nucleation of protein crystals: critical nuclei, phase behavior, and control pathways. *J. Cryst. Growth,* **2001**, *232*, 63-76.

[41] Yau, S.T.; Thomas, B.R.; Vekilov, P.G. Real time, in-situ, monitoring of apoferritin crystallization and defect formation with molecular resolution. *J. Cryst. Growth,* **2001**, *232*, 188-194.

[42] Yau, S.T.; Vekilov, P.G. Direct observation of nucleus structure and nucleation pathways in apoferritin crystallization. *J. Am. Chem. Soc.*, **2001**, *123*, 1080-1089.

[43] Sleutel, M.; Vanhee, C.; de Weerdt, C.V.; Decanniere, K.; Maes, D.; Willaert, L.W.R. The role of surface diffusion in the growth mechanism of triosephosphate isomerase crystals. *Cryst. Growth Des.*, **2008**, *8*, 1173-1180.

[44] Sazaki, G.; Matsui, T.; Tsukamoto, K.; Usami, N.; Ujihara, T.; Fujiwara, K.; Nakajima, K. In situ observation of elementary growth steps on the surface of protein crystals by laser confocal microscopy. *J. Cryst. Growth*, **2004**, *262*, 536-542.

[45] Sazaki, G.; Tsukamoto, K.; Yai, S.; Okada, M.; Nakajima, K. In situ observation of dislocations in protein crystals during growth by advanced optical microscopy. *Cryst. Growth Des.*, **2005**, *5*, 1729-1735.

[46] Van Driessche, A.E.S.; Otalora, F.; Gavira, J.A.; Sazaki, G. Is agarose an impurity or an impurity filter? In situ observation of the joint gel/impurity effect on protein crystal growth kinetics. *Cryst. Growth Des.*, **2008**, *8*, 3623-3629.

[47] Van Driessche, A.E.S.; Otalora, F.; Sazaki, G.; Sleutel, M.; Tsukamoto, K.; Gavira, J.A. Comparison of Different Experimental Techniques for the Measurement of Crystal Growth Kinetics. *Cryst. Growth Des.*, **2008**, *8*, 4316-4323.

[48] Van Driessche, A.E.S.; Sazaki, G.; Dai, G.L.; Otalora, F.; Gavira, J.A.; Matsui, T.; Yoshizaki, I.; Tsukamoto, K.; Nakajima, K. Direct Observation of Adsorption Sites of Protein Impurities and Their Effects on Step Advancement of Protein Crystals. *Cryst. Growth Des.*, **2009**, *9*, 3062-3071.

[49] Van Driessche, A.E.S.; Sazaki, G.; Otalora, F.; Gonzalez-Rico, F.M.; Dold, P.; Tsukamoto, K.; Nakajima, K. Direct and noninvasive observation of two-dimensional nucleation behavior of protein crystals by advanced optical microscopy. *Cryst. Growth Des.*, **2007**, *7*, 1980-1987.

[50] Dold, P.; Ono, E.; Tsukamoto, K.; Sazaki, G. Step velocity in tetragonal lysozyme growth as a function of impurity concentration and mass transport conditions. *J. Cryst. Growth*, **2006**, *293*, 102-109.

[51] Suzuki, Y.; Sazaki, G.; Matsumoto, M.; Nagasawa, M.; Nakajima, K.; Tamura, K. First Direct Observation of Elementary Steps on the Surfaces of Glucose Isomerase Crystals under High Pressure. *Cryst. Growth Des.*, **2009**, *9*, 4289-4295.

[52] Sleutel, M.; Maes, D.; Wyns, L.; Willaert, R. Kinetic Roughening of Glucose Isomerase Crystals. *Cryst. Growth Des.*, **2008**, *8*, 4409-4414.

[53] Sleutel, M.; Willaert, R.; Gillespie, C.; Evrard, C.; Wyns, L.; Maes, D. Kinetics and Thermodynamics of Glucose Isomerase Crystallization. *Cryst. Growth Des.*, **2009**, *9*, 497-504.

[54] Sleutel, M.; Willaert, R.; Wyns, L.; Maes, D. Polyhedral Instability of Glucose Isomerase Crystals. *Cryst. Growth Des.*, **2009**, *9*, 335-343.

[55] Funatsu, T.; Harada, Y.; Tokunaga, M.; Saito, K.; Yanagida, T. Imaging of Single Fluorescent Molecules and Individual Atp Turnovers by Single Myosin Molecules in Aqueous-Solution. *Nature*, **1995**, *374*, 555-559.

[56] Cognet, L.; Coussen, F.; Choquet, D.; Lounis, B. Fluorescence microscopy of single autofluorescent proteins for cellular biology. *Comptes Rendus Physique*, **2002**, *3*, 645-656.

[57] Kellermayer, M.S.Z. Visualizing and manipulating individual protein molecules. *Physiol. Meas.*, **2005**, *26*, R119-R153.

[58] Sako, Y.; Uyemura, T. Total internal reflection fluorescence microscopy for single-molecule imaging in living cells. *Cell. Struct. Funct.*, **2002**, *27*, 357-365.

[59] Wazawa, T.; Ueda, M. Total internal reflection fluorescence microscopy in single molecule nanobioscience. *Microscopy Techniques*, **2005**, *95*, 77-106.

[60] Dai, G.L.; Sazaki, G.; Matsui, T.; Tsukamoto, K.; Nakajima, K.; Kang, Q.; Hu, W.R. Gradual Immobilization Processes of Molecules during Transitions from Solute to Solid States. *Cryst. Growth Des.*, **2011**, *11*, 88-92.

[61] Sazaki, G.; Okada, M.; Matsui, T.; Watanabe, T.; Higuchi, H.; Tsukamoto, K.; Nakajima, K. Single-molecule visualization of diffusion at the solution - Crystal interface. *Cryst. Growth Des.*, **2008**, *8*, 2024-2031.

[62] Matsui, T.; Sazaki, G.; Hondoh, H.; Matsuura, Y.; Nakada, T.; Nakajima, K. Impurity effects of lysozyme molecules specifically labeled with a fluorescent reagent on the crystallization of tetragonal and monoclinic lysozyme crystals. *J. Cryst. Growth*, **2006**, *293*, 415-422.

[63] Konnert, J.H.; Dantonio, P.; Ward, K.B. Observation of Growth Steps, Spiral Dislocations and Molecular Packing on the Surface of Lysozyme Crystals with the Atomic-Force Microscope. *Acta Crystallogr. D*, **1994**, *50*, 603-613.

[64] Li, H.Y.; Nadarajah, A.; Pusey, M.L. Determining the molecular-growth mechanisms of protein crystal faces by atomic force microscopy. *Acta Crystallogr. D*, **1999**, *55*, 1036-1045.

[65] Van Driessche, A.E.S.; Garcia-Ruiz, J.M.; Delgado-Lopez, J.M.; Sazaki, G. In Situ Observation of Step Dynamics on Gypsum Crystals. *Cryst. Growth Des.*, **2010**, *10*, 3909-3916.

[66] Sazaki, G.; Zepeda, S.; Nakatsubo, S.; Yokoyama, E.; Furukawa, Y. Elementary steps at the surface of ice crystals visualized by advanced optical microscopy. *Proc. Natl. Acad. Sci. USA*, **2010**, *107*, 19702-19707.

[67] Sazaki, G.; Zepeda, S.; Nakatsubo, S.; Yokomine, M.; Furukawa, Y. Quasi-liquid layers on ice crystal surfaces are made up of two different phases. *Proc. Natl. Acad. Sci. USA*, **2012**, *109*, 1052-1055.

[68] Wen, R.; Lahiri, A.; Alagurajan, M.; Kuzume, A.; Kobayashi, S.; Itaya, K. Preparation and characterization of ultra-flat single crystal surfaces of Pd(1 1 1) and Au(1 1 1) by an in situ interference optical microscopy. *J. Electroanal. Chem.*, **2010**, *649*, 257-260.

[69] Wen, R.; Lahiri, A.; Azhagurajan, M.; Kobayashi, S.; Itaya, K. A New in Situ Optical Microscope with Single Atomic Layer Resolution for Observation of Electrochemical Dissolution of Au(111). *J. Am. Chem. Soc.*, **2010**, *132*, 13657-13659.

[70] Tsukamoto, K. In situ observation of mono-molecular growth steps on crystals growing in aqueous solution. *J. Crystal Growth*, **1983**, *61*, 199-209.

[71] Chernov, A.A. *Modern Crystallography III*. ed.; Springer-Verlag: Berlin, 1984; Vol. 36, p 127-129.

[72] Markov, I.V. *Crystal Growth for Beginners*. ed.; World Scientific Publishing: Singapore, 1995; p 192-197.

[73] Liu, X.Y.; Maiwa, K.; Tsukamoto, K. Heterogeneous two-dimensional nucleation and growth kinetics. *J. Chem. Phys.*, **1997**, *106*, 1870-1879.

[74] Toba, S.; Watanabe, T.M.; Yamaguchi-Okimoto, L.; Toyoshima, Y.Y.; Higuchi, H. Overlapping hand-over-hand mechanism of single molecular motility of cytoplasmic dynein. *Proc. Natl. Acad. Sci. USA*, **2006**, *103*, 5741-5745.

[75] Cheezum, M.K.; Walker, W.F.; Guilford, W.H. Quantitative comparison of algorithms for tracking single fluorescent particles. *Biophys. J.* **2001**, *81*, 2378-2388.

[76] Dubin, S.B.; Clark, N.A.; Benedek, G.B. *J. Chem. Phys.* **1971**, *54*, 5158-5164.

[77] Vaney, M.C.; Maignan, S.; Ries-Kautt, M.; Ducruix, A. High-resolution structure (1.33A) of a HEW lysozyme tetragonal crystal grown in the APCF apparatus. Data and structural comparison with a crystal grown under microgravity from SpaceHab-01 mission. *Acta Crystallogr. D*, **1996**, *52*, 505-517.

[78] Guesmi, H.; Lapena, L.; Ranguis, A.; Muller, P.; Treglia, G. Sb/Si(111) adsorption: Hidden phase transitions behind Langmuir-like isotherms. *Phys. Rev. Lett.*, **2005**, *94*, 076101(1-4).

[79] Nagaoka, H.; Imae, T. Analytical investigation of two-step adsorption kinetics on surfaces. *J. Colloid Interface Sci.*, **2003**, *264*, 335-342.

[80] Puskas, J.E.; Dahman, Y.; Margaritis, A. Novel thymine-functionalized polystyrenes for applications in biotechnology. 2. Adsorption of model proteins. *Biomacromolecules*, **2004**, *5*, 1412-1421.

[81] Thomas, B.R.; Vekilov, P.G.; Rosenberger, F. Heterogeneity determination and purification of commercial hen egg-white lysozyme. *Acta Crystallogr. D*, **1996**, *52*, 776-784.

[82] Cleveland, W.S. Robust Locally Weighted Regression and Smoothing Scatterplots. *J. Am. Stat. Assoc.*, **1979**, *74*, 829-836.

[83] Cleveland, W.S.; Devlin, S.J. Locally Weighted Regression - an Approach to Regression-Analysis by Local Fitting. *J. Am. Stat. Assoc.*, **1988**, *83*, 596-610.

[83] Cleveland, W.S.; Devlin, S.J. Locally Weighted Regression - an Approach to Regression-Analysis by Local Fitting. *J. Am. Stat. Assoc.*, **1988**, *83*, 596-610.
[84] Bliznakov, G. *Fortschritte der Mineralogie*, **1958**, *36*, 149-191.
[85] Cabrera, N.; Vermilyea, D.A. Growth and Perfection of Crystals. In: *Growth and Perfection of Crystals, Proceedings*, Doremus, R.H.; Roberts, B.W.; Turnbull, D., Eds.; John Wiley & Sons: New York, **1958**; pp 393-410.
[86] Sangwal, K. *Additives and Crystallization Processes: From Fundamentals to Applications*. ed.; John Wiley & Sons: West Sussex, **2007**.
[87] Sangwal, K. Effects of impurities on crystal growth processes. *Progress in Crystal Growth and Characterization of Materials*, **1996**, *32*, 3-43.
[88] van der Eerden, J.P. In: *Handbook of Crystal Growth 1: Fundamentals*, Hurle, D.T.J., Ed.; North-Holland: Amsterdam, **1993**; Vol. 1a, pp 307-479.

**Received: July 8, 2011** **Revised: July 27, 2011** **Accepted: February 11, 2012**